Final Version NCHEM-17061131.

Enzyme-powered motility in buoyant organoclay/DNA protocells

B.V.V.S. Pavan Kumar, Avinash J. Patil,* and Stephen Mann*

Centre for Protolife Research and Centre for Organized Matter Chemistry, School of Chemistry, University of Bristol, Bristol BS8 1TS, UK.
*e-mail: avinash.patil@bristol.ac.uk; s.mann@bristol.ac.uk

Reconstitution and simulation of cellular motility in micro-compartmentalized colloidal objects have important implications for microcapsule-based remote sensing, environmentally induced signaling between artificial cell-like entities, and programming spatial migration in synthetic protocell consortia. Here, we describe the design and construction of catalase-containing organoclay/DNA semipermeable microcapsules, which in the presence of hydrogen peroxide exhibit enzyme-powered oxygen gas bubble-dependent buoyancy. We determine the optimum conditions for single/multiple bubble generation per microcapsule, monitor the protocell velocities and resilience, and use remote magnetic guidance to establish reversible changes in buoyancy. Co-encapsulation of catalase and glucose oxidase is exploited to establish a spatiotemporal response to antagonistic bubble generation and depletion to produce protocells capable of sustained oscillatory vertical movement. We demonstrate that the motility of the microcapsules can be used for the flotation of macroscopic objects, self-sorting of mixed protocell communities, and delivery of a biocatalyst from an inert to chemically active environment. These results highlight new opportunities for constructing programmable micro-compartmentalized colloids with buoyancy-derived motility.

Introduction

Directional motility or 'taxis' is a key feature of microbial life that enables the realization of diverse cellular functions through access to favorable environments. Microorganisms have evolved a high degree of control over their locomotion using motility mechanisms that range from simple gliding and gas vesicle-mediated buoyancy to complex flagella-based movements.[1] Reconstitution and simulation of these cellular motility functions into synthetic protocellular models have important implications for the environmentally induced signaling and triggering of protometabolic networks, establishing self-organization in protocell communities, and providing mechanisms for long-range collective behavior. Installing locomotive mechanisms in synthetic objects is highly challenging, and although the study of biological motor proteins in artificial micro-compartments is being addressed,[2, 3] most studies are primarily based on the development of artificial micro/nano-scale motors.[4, 5] In this regard, several approaches have been investigated: (i) motors powered by electrical,[6] magnetic,[7, 8] light[9, 10] or acoustic[11, 12] external

force fields that exhibit directionality or intentional motility; (ii) motors driven by chemical reactions at interfaces that generally exhibit chaotic trajectories;[13-17] and (iii) hybrid motors powered by chemical reactions and guided by external force fields.[18-20]

Whilst artificial motors have been successfully applied to solid objects such as nanorods and colloidal beads, implementation of these strategies in nano- or micro-compartmentalized structures has not been extensively investigated. Bubble propulsion arising from Pt-catalysed oxygen production has been successfully employed as a mechanism to mobilize nano- or micro-compartments across chaotic/random trajectories by asymmetric placement of the metal catalyst[21] or asymmetric release of bubbles,[22] respectively. Wilson *et al.* have illustrated directional motility in nanocapsules (stomatocytes) either under the influence of gradients of hydrogen peroxide[23] (chemotaxis) generated by neutrophil cells, or under magnetic guidance[24] (magnetotaxis) by employing a Ni-Pt catalyst to steer the nanocapsules through a model tissue while being propelled by decomposition of hydrogen peroxide. Lu *et al.* have also demonstrated directional motility in Fe-Pt nanoparticle-loaded microcapsules propelled by Pt-catalysed oxygen production under remote magnetic guidance to pick-up and drop-off microscale cargo.[25] Nanoscopic[26-28] and microscopic[29, 30] compartments have also been powered by enzymatic transformations[31, 32] to achieve mostly random trajectories unless directed by magnetic manipulation.[30] For example, single-enzyme mediated transformations have been used to power the motion of silica-based nano-[28] and micro-[30] capsules and polyelectrolyte microcapsules[29] by the asymmetric surface attachment of enzymes onto the capsule surface. Enzyme cascades have been employed to power the motion of nanocapsules[27] and attain sustained autonomous movement[26] albeit in random trajectories.

Implementation of the above strategies to synthetic protocell models based on microscale water-filled biomimetic compartments such as lipid vesicles, emulsion droplets, proteinosomes and colloidosomes has not been widely explored. Chaotic motions have been demonstrated in reactive oil droplet/water protocell models[33] that exhibit chemotactic[34] or phototactic[35, 36] responses but are constrained by their biphasic nature. Enabling directional movement in protocellular models therefore remains a considerable challenge and places a serious constraint on designing complex interactions within synthetic protocell communities for the programming of emergent and collective behavior.[37, 38] As a step towards a rudimentary model of motility in communities of synthetic protocells, herein we describe a buoyancy-mediated mechanism of locomotion that is inspired by the operation of gas vesicles in cyanobacteria.[39] The following design principles were employed to generate a protocell model capable of buoyancy-derived motility: (i) facile self-assembly of membrane-delineated micro-compartments with sufficient size and structural robustness to house the nucleation, growth and stabilization of gas micro-bubbles specifically within an aqueous-filled lumen; (ii) encapsulation of surface-active macromolecules within the lumen to preferentially stabilize the developing bubble/water interface; (iii) encapsulation of a gas-generating pathway to trigger the local

supersaturation of dissolved gas required for preferential nucleation of the bubble within but not outside the micro-compartment; (iv) provision of a reconfigurable, elastic membrane to dissipate the volumetric stress associated with high rates of bubble growth from slightly supersaturated solutions (typically, *ca.* 100 μm/min)[40] and re-establish structural integrity after release of the encapsulated bubbles at the air/water interface; (v) co-encapsulation of a complementary gas-consuming pathway to enable dynamic control of bubble size via *in situ* downsizing to sediment the microcapsules under the influence of gravity and generate protocells exhibiting reversible buoyancy.

To meet the above criteria, herein we describe the use of self-assembled "giant" organoclay/DNA semi-permeable microcapsules as a novel chassis for the design and construction of reversibly buoyant protocells that are enzymatically powered in the presence of encapsulated catalase (Fig. 1). We specifically use the organoclay/DNA microcapsules because the reproducible nucleation and growth of stable gas bubbles in other protocell models such as colloidosomes,[41,42] proteinosomes,[43] coacervates[44] or lipid vesicles[45, 46] was found to be unsuccessful due to the smaller size of these micro-compartments or inelasticity of their membranes, or both. The organoclay/DNA microarchitectures are fabricated by electrostatically induced complexation at the surface of aqueous *ds*DNA/catalase droplets suspended in a dispersion of ultrathin sheets of a cationic synthetic organoclay.[47] Subsequent addition of hydrogen peroxide promotes the catalase-mediated formation of oxygen bubbles, which reside specifically within the protocells due to the large size of the microcapsules, elasticity of the organoclay/DNA membrane and surface-active properties of the encapsulated solution of non-complexed *ds*DNA and catalase. As a consequence, the synthetic protocells exhibit enzyme-mediated buoyancy. We determine the optimum conditions for single or multiple bubble generation per microcapsule, monitor the protocell velocities and resilience as a function of bubble volume and areal strain, respectively, and use remote magnetic guidance to establish reversible changes in buoyancy. Significantly, we construct organoclay/DNA microcapsules capable of sustained oscillatory movement by co-encapsulation of catalase and glucose oxidase (GOx), which together provide antagonistic regulation of oxygen bubble generation and consumption within the protocells. Finally, we exploit the buoyancy properties at the population level for the flotation of macroscopic objects, segregation of mixed protocell communities, and delivery of a biocatalyst from a passive to chemically active environment.

Results and Discussion

General properties of organoclay/DNA microcapsules for protocell modelling

Organoclay/DNA microcapsules with diameters in the range of 300-400 μm were prepared by extrusion of droplets of aqueous *ds*DNA (2 mg/mL, M_W ≈ 1300 kDa, salmon testes) into an aqueous dispersion of exfoliated aminopropyl-functionalised magnesium phyllosilicate (AMP) clay sheets (5 mg/mL) using an extrusion speed of 10 μL/min and air-flow rate of 2.5 L/min (Fig.

2a). The size of the microcapsules was varied by adjusting the rate of DNA extrusion, diameter of the hypodermic needle or rate of the shearing airflow. Under a given set of conditions, the polydispersity in microcapsule size was low (typically, PDI = 1.004; n = 35). In general, the organoclay/DNA microstructures were able to withstand temperatures up to 90°C and reversibly undergo mechanical deformation at low compression forces (Supplementary Fig. 1). Intact microcapsules were not readily produced when the DNA concentration was decreased below 1 mg/mL due to the reduced viscosity of the DNA solution prepared under these conditions. Optical microscopy images indicated that the microcapsules consisted of an aqueous DNA lumen surrounded by a continuous organoclay/DNA membrane. Images of acridine orange-stained DNA trapped within the capsules revealed that the free DNA was essentially impermeable to the membrane (Fig. 2b). The thickness of the organoclay/DNA membrane was estimated from fluorescence optical microscopy images and associated fluorescence intensity profiles of microcapsules stained with the anionic dye pyranine, which strongly adsorbed to the cationic organoclay sheets entangled within the hybrid shell (Fig. 2c). Shell thicknesses of 3-5 μm were typically observed. CD spectroscopy confirmed that the DNA helicity and melting temperature (35-45°C) were effectively unchanged after encapsulation or complexation with the organoclay sheets (Supplementary Fig. 2 and Supplementary Fig. 3).

To assess the potential of the organoclay/DNA microcapsules as a novel protocell model, we investigated the permeability of the hybrid membrane, scope for inducing structuration within the DNA-enriched aqueous lumen, and ability to regulate enzyme-mediated reactions within the micro-compartments. Studies on the passive uptake and release of a range of molecules indicated that the organoclay/DNA membrane was semi-permeable depending on the molecular weight of the solute (Fig. 4). As a consequence, addition of excess glucose to the external solution produced a temporary hypertonicity that resulted in an osmotic pressure-induced shrinkage of the microcapsules followed by relaxation back to their original shape within 15 minutes as the glucose concentration equilibrated across the organoclay/DNA membrane (Supplementary Fig. 5). In contrast, addition of carboxymethyldextran (M_w = 10-20 kDa) to the external solution resulted in a permanent hypertonicity that caused the microcapsules to shrink irreversibly, suggesting that the permeability limit was less than 20 kDa (Fig. 2d and Supplementary Fig. 6). The deflated microcapsules remained structurally intact and could be inflated as intact microstructures by eliminating the osmotic gradient, indicating that the membrane was sufficiently elastic to withstand considerable changes in shape and size. Selective uptake of cationic dyes such as acridine orange, methylene blue and rhodamine 6G into the aqueous lumen of the microcapsules was observed typically within 5-10 min (Fig. 2e,f and Fig. 7), whilst anionic dyes such as pyranine and tetraphenylporphine sulfonate were sequestered into the membrane and did not transfer into the aqueous DNA-containing lumen (see Fig. 2c and Fig. 7). By comparison, high molecular weight solutes such as rhodamine-labeled bovine serum albumin (RITC-BSA) could not cross the membrane, resulting in efficient levels of exclusion or

encapsulation (Supplementary Fig. 8). Similarly, capsid-like proteins such as ferritin, micrometer-sized magnetic polymer beads, calcium carbonate particles and fluorescent silica particles could be encapsulated and retained within the hybrid micro-compartments (Fig. 2g and Supplementary Fig. 9). Significantly, we were also able to fabricate organoclay/DNA capsules that contained cross-linked silica colloidosomes prepared as described previously (Fig. 2h and Fig. 10).[41] As the colloidosomes have been extensively investigated as synthetic protocells,[42, 48, 49] the ability to capture these micro-compartmentalized colloidal objects within the organoclay/DNA microcapsules offers a potential route towards hierarchically organized protocell micro-architectures with spatially distributed functions and nested properties.

We exploited the selective membrane properties of the organoclay/DNA microcapsules as a mechanism for inducing structuration within the confined aqueous lumen. For this, we added the cationic peptide protamine ($M_w \approx 5.1$ kDa) to the continuous phase of an aqueous dispersion of microcapsules such that uptake of the peptide and complexation with free DNA molecules gave rise to the self-assembly of a condensed peptide/DNA phase within the micro-compartment interior after approximately 10 min. Fluorescence optical microscopy images of samples stained with acridine orange showed the presence within each microcapsule of a discrete membrane-free condensate that was intricately connected to the organoclay/DNA membrane by a network of filaments (Fig. 2i). Condensation of the DNA molecules had no effect on membrane structure or the structural integrity of the microcapsules. These preliminary observations suggest that the formation of a peptide/DNA coacervate within the microcapsules could provide a step towards the development of a synthetic protocell comprising an "artificial nucleus" capable of storing and processing genetic information, for example via controlled complexation/decomplexation processes coupled to *in vitro* methods of transcription and translation.[50]

Based on the observed uptake and retention properties of various substrate molecules, we tested whether enzyme-mediated transformations could be undertaken within the DNA-rich environment of the organoclay/DNA microcapsules. As proof of concept, we encapsulated alkaline phosphatase (ALP) within the micro-compartments and added various amounts of *p*-nitrophenylphosphate to the external medium, and monitored the formation of the dephosphorylated product *p*-nitrophenol at room temperature by measuring changes in absorption at 410 nm. The results indicated that enzyme activity was retained within the organoclay/DNA microcapsules (Supplementary Fig. 11). Dephosphorylation occurred via passive diffusion of the substrate through the organoclay/DNA membrane and was observed to take place even when the Mg^{2+} cofactor was not added to the reaction mixture due to *in situ* leaching of the divalent cation from the organoclay matrix.

Buoyancy-induced motility in catalase-containing organoclay/DNA protocells

Given the above range of biomimetic properties, we encapsulated catalase within the organoclay/DNA microcapsules as a step towards the fabrication of enzyme-powered motile protocells (Fig. 3a,b). An aqueous dispersion of the microcapsules was allowed to sediment in a

quartz cuvette and then hydrogen peroxide was added. Optical microscopy images revealed that single or multiple bubbles of oxygen were produced inside the microcapsules within a minute after addition of the enzyme substrate. The bubbles appeared as discrete spherical microstructures that were optically dark and increased in size with time but remained spatially entrapped within the protocells. As a consequence, the organoclay/DNA microcapsules were able to harness the buoyant force to move against gravity such that they rapidly migrated from their resting position at the bottom of the cuvette to the air/water interface (Supplementary video 1). Typically, greater than 98% of the protocell population displayed buoyancy-induced motility when prepared with a catalase concentration of 39 KU/mL and exposed to >15 mM hydrogen peroxide. The microcapsules moved at terminal velocities of up to 40 mm s^{-1} and exhibited rectilinear trajectories associated with the buoyant force (Fig. 3c). The nucleated oxygen bubbles were initially free to diffuse through the interior of the microcapsules but as they enlarged became immobilized on the organoclay/DNA membrane at the top of the protocells, which resulted in upward motion (Fig. 3d)**.** Further growth of the entrapped bubbles along with additional nucleation events were also observed as the microcapsules ascended to the air/water interface (Fig. 3d), indicating that the motile protocells remained enzymatically active. Under these conditions, the continuous change in the buoyant force prevented the protocells from reaching terminal velocity during the time required to transit the height of the water column, typically travelling at velocities < 10 mm s^{-1} (Supplementary Fig. 12). In contrast, by minimizing enzyme activity during transit to the air/water interface by physically delaying the onset of buoyancy such that microbubble growth was essentially completed prior to upward movement, we were able to attain terminal velocities during the transit time (Supplementary Fig. 12), as well as map these values against the volume of the encapsulated oxygen bubbles. The normalized velocity profiles showed a rapid initial rise in velocity with gradual saturation to reach a terminal velocity within 0.2-0.4 s (Fig. 3e). The terminal velocities ranged from 10 to 40 mm s^{-1} and increased with the size of the entrapped microbubbles, which were typically between 260-490 μm in diameter. Plots of terminal velocity against entrapped bubble volume gave a linear relationship (Fig. 3f), consistent with previous observations on gas bubbles in this size regime.[51]

The probability of bubble nucleation within the organoclay/DNA microcapsules was investigated by systematically varying both the activity of the encapsulated catalase and added hydrogen peroxide concentration. Three different regimes were observed in which gas bubbles were either produced outside the microcapsules, or single, dual or multiple oxygen bubbles nucleated and entrapped within the protocells (Fig. 4a). Changing the enzyme and substrate concentrations had a marked influence on the nucleation probability (Fig. 4b). At low concentrations of either catalase or hydrogen peroxide, less than 10 % of the protocells were buoyant, and most of the gas bubbles were produced outside the protocells. Increasing the enzyme and substrate concentrations to values of between 2-10 KU/mL and 7-30 mM, respectively, resulted in buoyant protocells comprising single gas bubbles in up to 80% of the

population (Fig. 4c and Supplementary Fig. 13). In contrast, two or more gas bubbles were produced and entrapped within increasing numbers of the buoyant microcapsules when the enzyme concentration was increased to approximately 40 KU/mL at hydrogen peroxide concentrations > 10 mM (Fig. 4c and Supplementary Fig. 13).

Using image analysis, we monitored changes in the total microcapsule volume as well as the volume of the internally trapped DNA/catalase liquid during growth of single gas bubbles within the protocells (Fig. 4d,e). Expansion of the gas bubble resulted in a concomitant increase in the size of the capsules, along with a contraction in the volume occupied by the entrapped aqueous solution. Although the entrapped liquid phase was progressively reduced to less than half of the initial volume, no release of the macromolecular contents was observed (Supplementary video 2). The results implied that water was extruded from the protocell via a process of reverse osmosis in which the volumetric stress generated by the bubble pushing against the semipermeable organoclay/DNA membrane was sufficient to force water out of the microcapsule. In this regard, the microcapsules were remarkably tolerant to the expansive strain produced by the growing gas bubbles, with more than 50% of the population (9 out of 16 microcapsules) remaining intact when the surface area was increased three-fold (Fig. 4f). Indeed, the catalase-containing microcapsules were observed to grow to almost six times their initial volume before rupturing of the membrane obliterated the protocell population (Fig. 4d,f and Supplementary Video 3). The ability of the membrane to undergo distension and dynamic reconfiguration under stress was attributed to the viscoelastic nature of the entangled organoclay/DNA shell and the reversibility of the electrostatic interactions between the cationic organoclay sheets and negatively charged DNA polyelectrolyte.

Enzyme-powered oscillatory movement in organoclay/DNA capsules

Having established optimal conditions for the catalase-mediated buoyancy of organoclay/DNA microcapsules, we used an encapsulated oxygen-dependent enzyme cascade to produce populations of protocells capable of reversible buoyancy and sustained oscillatory movement. For this, catalase and GOx were co-encapsulated within the microcapsules and hydrogen peroxide or glucose used to trigger or override the buoyant force, respectively (Fig. 5a,b). As GOx-mediated oxidation of glucose requires dioxygen, we sought to use this reaction as a mechanism for consuming the entrapped oxygen bubbles present in the ascending protocells, thereby inducing the microcapsules to descend under gravity in the water column. As the catalase and GOx reactions have stoichiometries of 0.5 mole/substrate (O_2 production) and 1.0 mole/substrate (O_2 consumption), oxygen depletion is favoured under competitive conditions (Fig. 5c and Supplementary Fig. 14). To generate multiple oscillations, we employed a specially designed apparatus to control the delivery of continuous flows of glucose and hydrogen peroxide to the top and bottom of the water column, respectively (Fig. 5d and Supplementary Fig. 15). As a consequence, oscillations in the vertical displacement of the capsules could be sustained for

extended periods of time (4-5 h) (Fig 5e,f; Supplementary Fig. 16 and S17; supplementary video 4). Typically, the capsules ascended with an average speed of ca. 1 mm s^{-1}, which was approximately three times faster than the speed of descent (0.3 mm s^{-1}). The periodicity of the oscillations was 8-13 min, and the residence times at the bottom and top of the water column due to the lag time associated with the switch between oxygen generation and consumption were *ca*. 1 min and 2-4 min, respectively. Variations in periodicity and residence times were attributed to stochastic events associated with the intersection of individual capsule trajectories during ascent and descent, and the number of capsules transiently located at each end of the water column (changes in enzyme substrate competition).

The above results indicate that oscillatory movement of a population of organoclay/DNA capsules can be established by the spatiotemporal response of oxygen-dependent antagonistic enzymes housed within cascade reaction. To generate oscillatory behavior with shorter time periods, we employed an external magnetic field to offset the buoyancy such that rapid non-diffusive changes in motility could be readily established by remote guidance. For this, we encapsulated magnetic polymer microparticles within the catalase-containing organoclay/DNA microcapsules (Fig. 5g), and added hydrogen peroxide to generate a buoyant force, which was then magnetically manipulated by placing or removing a magnet beneath the cuvette (Fig. 5h). As the magnetic force could be tuned by varying the magnetic field strength and amount of magnetic particles encapsulated within the protocells, sustained oscillations in vertical trajectory could be readily achieved depending on whether the magnetic force was stronger or weaker than the buoyant force (Fig. 5i and Supplementary video 5).

Buoyancy-induced properties of organoclay/DNA protocell populations

As a step towards developing rudimentary modes of coordinated behaviour in populations of motile synthetic protocells, we exploited the buoyancy properties of catalase-containing organoclay/DNA microcapsules at the population level for the flotation of macroscopic objects, segregation of mixed protocell communities, and inducing “niche” transitions between different chemical environments.

The striking ability of the organoclay/DNA microcapsules to accommodate large amounts of oxygen gas equivalent to up to six times the initial volume without membrane rupture was used to generate a buoyant force large enough to drive the vertical displacement of a macroscopic object. Specifically, we placed a large population (*ca*. 225 protocells) of the catalase-containing organoclay/DNA microcapsules within a submerged dialysis bag (3-4 cm in length), sealed the bag and placed it at the bottom of a measuring cylinder containing 100 mL of water (Fig. 6a). Addition of hydrogen peroxide, and the corresponding nucleation and growth of gas bubbles within the individual capsules resulted in the flotation of the dialysis bag over a period of 7 min reaching velocities of *ca*. 15 mm s^{-1} (Fig. 6b and Supplementary video 6). Similarly, we were able to use the high buoyant force to disassociate a heterogeneously mixed population of

catalase-containing organoclay/DNA microcapsules and silica colloidosomes produced by co-sedimentation in a cuvette (Fig. 6c). Addition of hydrogen peroxide to the binary population resulted in nucleation and growth of oxygen bubbles specifically in the organoclay/DNA microcapsules buried within the colloidosome community (Fig. 6d). As a consequence, the buoyant force was sufficient to move the organoclay/DNA microcapsules through the dense matrix of colloidosomes and eject them into the solution at upward speeds up to 40 mm s^{-1} (Fig. 6e,f and Supplementary Video 7). In this way, the binary population was spatially segregated into two compositionally distinct protocell populations within a period of approximately 3 min.

Finally, as a step towards the notion of how synthetic protocells might access different artificial niches, we used enzyme-powered buoyancy to transfer a population of motile organoclay/DNA microcapsules from an inert to chemically active environment. The movement of the buoyant microcapsules was utilized to generate migration of the population towards a substrate-laden surface where an enzyme within the protocells metabolized the substrate to simulate a primitive chemical feeding mechanism (Fig. 6g). Specifically, we prepared organoclay/DNA microcapsules with co-encapsulated catalase and ALP enzymes (Fig. 6h), and placed the community 18 mm below a suspended agarose gel containing a colorless phosphorylated substrate (phenolphthalein bisphosphate, PPBP) in a buffered medium at pH 9. Addition of hydrogen peroxide resulted in migration towards the agarose gel, and accumulation of the protocells at the gel surface gave rise to ALP-mediated dephosphorylation of PPBP and localized production of phenolphthalein, as observed by the onset of a pink coloration initially within the protocells (Supplementary video 8). Within five minutes, the coordinated activity of the transferred protocells resulted in release of phenolphthalein into the aqueous solution adjacent to the polysaccharide gel as well as into the near surface regions of the agarose matrix (Fig. 6i and Supplementary Fig. 18). Control experiments undertaken in the absence of hydrogen peroxide showed no migration of the protocells and no development of pink color in the aqueous solution or agarose gel even after 20 minutes.

Conclusions

In this article, we demonstrate that self-assembled “giant” organoclay/DNA microcapsules are capable of guest molecule encapsulation, selective permeability, elastic deformation, peptide-induced structuration, hierarchical structuration, and multiple enzymatic transformations. Significantly, we show that buoyancy-induced motility can be generated in catalase-containing organoclay/DNA protocells by enzyme-mediated production of entrapped oxygen gas bubbles in the presence of hydrogen peroxide. Motilities with rectilinear trajectories and velocities reaching up to 40 mm s^{-1} are observed, and can be offset by competing GOx-mediated consumption of the entrapped bubbles to produce capsules capable of sustained oscillatory movement in the vertical direction. Moreover, at the population level, the enzyme-powered buoyancy can be exploited to achieve self-sorting in mixed protocell communities, vertical transportation of macroscopic

objects, and migration of enzymatically active protocells between different chemical environments. In the latter case, we demonstrate that remote chemical milieu can be accessed and processed by transiting of the buoyant microcapsules under substrate regulation, suggesting that it should be possible to develop this strategy for more complex protocell behaviours.

For example, oscillatory motion of the buoyant protocells could be used to transfer the motile microcapsules in and out of light- or dark-rich zones established in the upper and lower layers of a water column, respectively. In so doing, it should be feasible to couple the enzyme-powered buoyancy to the triggering of photo-induced processes within the protocells to establish a rudimentary form of phototrophic behavior. Furthermore, the oscillatory motion of the buoyant protocells could be used to develop strategies for microcapsule-based logistics or chaperone-like behavior in which designated payloads such as functional microparticles, drug molecules or different types of synthetic protocells (and living cells?) are captured, co-transported and released across light/dark interfaces or different chemical fields. Finally, in the longer term, it may be possible to couple energy gradients in the water column to enzyme-powered buoyancy such that complex collective and emergent behaviors are established amongst consortia of synthetic protocells by establishing distinct spatial pathways between physically segregated communities of micro-compartmentalized colloidal objects.

Data availability

The authors declare that all relevant data supporting the finding of this study are available within the paper and its supplementary information files. Additional data are available from the corresponding author upon request.

Acknowledgements

We thank the EPSRC, ERC Advanced Grant Scheme, BrisSynBio, Marie-Curie Individual Fellowship (B.V.V.S.P.K) and University of Bristol (A.J.P.) for financial support, Duncan Tarling for assistance with fabrication of specifically designed glassware, Dr Liangfei Tian for useful discussions and Drs Mei Li, David S. Williams and Ravinash Krishna Kumar for assistance with preliminary experiments.

Author contributions

B.V.V.S.P.K., A.J.P. and S.M. conceived the experiments; B.V.V.S.P.K. and A.J.P. performed the experiments; B.V.V.S.P.K., A.J.P. and S.M. undertook data analysis; B.V.V.S.P.K., A.J.P. and S.M. wrote the manuscript.

Corresponding authors

Correspondence and requests for materials should be addressed to Avinash J. Patil or Stephen Mann.

Competing financial interests

The authors declare no competing financial interests.

References

1. Jarrell K. F. & McBride M. J. The surprisingly diverse ways that prokaryotes move. *Nat. Rev. Microbiol.* **6,** 466-476 (2008).

2. Herold C., Leduc C., Stock R., Diez S. & Schwille P. Long-range transport of giant vesicles along microtubule networks. *ChemPhysChem* **13,** 1001-1006 (2012).

3. Bottier C. *et al.* Active transport of oil droplets along oriented microtubules by kinesin molecular motors. *Lab Chip* **9,** 1694-1700 (2009).

4. Sánchez S., Soler L. & Katuri J. Chemically powered micro- and nanomotors. *Angew. Chem. Int. Ed.* **54,** 1414-1444 (2015).

5. Guix M., Mayorga-Martinez C. C. & Merkoçi A. Nano/micromotors in (bio)chemical science applications. *Chem. Rev.* **114,** 6285-6322 (2014).

6. Loget G. & Kuhn A. Electric field-induced chemical locomotion of conducting objects. *Nat. Commun.* **2,** 535 (2011).

7. Dreyfus R. *et al.* Microscopic artificial swimmers. *Nature* **437,** 862-865 (2005).

8. Ghosh A. & Fischer P. Controlled propulsion of artificial magnetic nanostructured propellers. *Nano Lett.* **9,** 2243-2245 (2009).

9. Ibele M., Mallouk T. E. & Sen A. Schooling behavior of light-powered autonomous micromotors in water. *Angew. Chem. Int. Ed.* **48,** 3308-3312 (2009).

10. Hong Y., Diaz M., Córdova-Figueroa U. M. & Sen A. Light-driven titanium-dioxide-based reversible microfireworks and micromotor/micropump systems. *Adv. Funct. Mater.* **20,** 1568-1576 (2010).

11. Wang W. *et al.* Acoustic propulsion of nanorod motors inside living cells. *Angew. Chem.* **126,** 3265-3268 (2014).

12. Wang W., Castro L. A., Hoyos M. & Mallouk T. E. Autonomous motion of metallic microrods propelled by ultrasound. *ACS Nano* **6,** 6122-6132 (2012).

13. Paxton W. F. *et al.* Catalytic nanomotors : Autonomous movement of striped nanorods. 13424-13431 (2004).

14. Howse J. R. *et al.* Self-motile colloidal particles: From directed propulsion to random walk. *Phys. Rev. Lett.* **99,** 048102 (2007).

15. Vicario J. *et al.* Catalytic molecular motors : Fuelling autonomous movement by a surface bound synthetic manganese catalase. *Chem. Commun.* **0,** 3936-3938 (2005).

16. Pantarotto D., Browne W. R. & Feringa B. L. Autonomous propulsion of carbon nanotubes powered by a multienzyme ensemble. *Chem. Commun.* **0,** 1533-1535 (2008).

17. Schattling P., Thingholm B. & Städler B. Enhanced diffusion of glucose-fueled janus particles. *Chem. Mater.* **27,** 7412-7418 (2015).

18. Solovev A. A., Smith E. J., Bof ' Bufon C. C., Sanchez S. & Schmidt O. G. Light-controlled propulsion of catalytic microengines. *Angew. Chem. Int. Ed.* **50,** 10875-10878 (2011).

19. Baraban L. *et al.* Catalytic janus motors on microfluidic chip: Deterministic motion for targeted cargo delivery. *ACS Nano* **6,** 3383-3389 (2012).

20. Xu T. *et al.* Reversible swarming and separation of self-propelled chemically powered nanomotors under acoustic fields. *J. Am. Chem. Soc.* **137,** 2163-2166 (2015).

21. Krishna Kumar R., Yu X., Patil A. J., Li M. & Mann S. Cytoskeletal-like supramolecular assembly and nanoparticle-based motors in a model protocell. *Angew. Chem. Int. Ed.* **50,** 9343-9347 (2011).

22. Wilson D. a., Nolte R. J. M. & van Hest J. C. M. Autonomous movement of platinum-loaded stomatocytes. *Nat. Chem.* **4,** 268-274 (2012).

23. Peng F., Tu Y., van Hest J. C. M. & Wilson D. A. Self-guided supramolecular cargo-loaded nanomotors with chemotactic behavior towards cells. *Angew. Chem. Int. Ed.* **54,** 11662-11665 (2015).

24. Peng F., Tu Y., Men Y., van Hest J. C. M. & Wilson D. A. Supramolecular adaptive nanomotors with magnetotaxis behavior. *Adv. Mater.* **29,** 1604996 (2017).

25. Lu A. X. *et al.* Catalytic propulsion and magnetic steering of soft, patchy microcapsules: Ability to pick-up and drop-off microscale cargo. *ACS Appl. Mater. Interaces* **8,** 15676-15683 (2016).

26. Nijemeisland M., Abdelmohsen L. K. E. A., Huck W. T. S., Wilson D. A. & van Hest J. C. M. A compartmentalized out-of-equilibrium enzymatic reaction network for sustained autonomous movement. *ACS Cent. Sci.* **2,** 843-849 (2016).

27. Abdelmohsen L. K. E. A. *et al.* Dynamic loading and unloading of proteins in polymeric stomatocytes: Formation of an enzyme-loaded supramolecular nanomotor. *ACS Nano* **10,** 2652-2660 (2016).

28. Ma X. *et al.* Enzyme-powered hollow mesoporous janus nanomotors. *Nano Lett.* **15,** 7043-7050 (2015).

29. Wu Y., Lin X., Wu Z., Möhwald H. & He Q. Self-propelled polymer multilayer janus capsules for effective drug delivery and light-triggered release. *ACS Appl. Mater. Interaces* **6,** 10476-10481 (2014).

30. Ma X., Wang X., Hahn K. & Sánchez S. Motion control of urea-powered biocompatible hollow microcapsules. *ACS Nano* **10,** 3597-3605 (2016).

31. Ma X., Hortelão A. C., Patiño T. & Sánchez S. Enzyme catalysis to power micro/nanomachines. *ACS Nano* **10,** 9111-9122 (2016).

32. Ortiz-Rivera I., Courtney T. M. & Sen A. Enzyme micropump-based inhibitor assays. *Adv. Funct. Mater.* **26,** 2135-2142 (2016).

33. Lach S. *et al.* Tactic, reactive, and functional droplets outside of equilibrium. *Chem. Soc. Rev.* **65,** 1392-1399 (2016).

34. Hanczyc M. M., Toyota T., Ikegami T., Packard N. & Sugawara T. Fatty acid chemistry at the oil−water interface: Self-propelled oil droplets. *J. Am. Chem. Soc.* **129,** 9386-9391 (2007).

35. Ichimura K., Oh S.-K. & Nakagawa M. Light-driven motion of liquids on a photoresponsive surface. *Science* **288,** 1624-1626 (2000).

36. Tang X. *et al.* Photochemically induced motion of liquid metal marbles. *Appl. Phys. Lett.* **103,** 174104 (2013).

37. Qiao Y., Li M., Booth R. & Mann S. Predatory behaviour in synthetic protocell communities. *Nat. Chem.* **9,** 110-119 (2017).

38. Rodriguez-Arco L., Li M. & Mann S. Phagocytosis-inspired behaviour in synthetic protocell communities of compartmentalized colloidal objects. *Nat. Mater.* **16,** 857-863 (2017).

39. Pfeifer F. Distribution, formation and regulation of gas vesicles. *Nat. Rev. Microbiol.* **10,** 705-715 (2012).

40. Enríquez O. R. *et al.* Growing bubbles in a slightly supersaturated liquid solution. *Rev. Sci. Instrum.* **84,** 065111 (2013).

41. Li M., Green D. C., Anderson J. L. R., Binks B. P. & Mann S. In vitro gene expression and enzyme catalysis in bio-inorganic protocells. *Chem. Sci.* **2,** 1739 (2011).

42. Li M., Harbron R., Weaver J., Binks B. & Mann S. Electrostatically gated membrane permeability in inorganic protocells. *Nat. Chem.* **5,** 529-536 (2013).

43. Huang X. *et al.* Interfacial assembly of protein-polymer nano-conjugates into stimulus-responsive biomimetic protocells. *Nat. Commun.* **4,** 2239 (2013).

44. Koga S., Williams D. S., Perriman A. W. & Mann S. Peptide-nucleotide microdroplets as a step towards a membrane-free protocell model. *Nat. Chem.* **3,** 720-724 (2011).

45. Szostak J. W., Bartel D. P. & Luisi P. L. *Nature* **409,** 387-390 (2001).

46. Walde P. & Ichikawa S. Enzymes inside lipid vesicles: Preparation, reactivity and applications. *Biomol. Eng.* **18,** 143-177 (2001).

47. Datta K. K. R., Achari a. & Eswaramoorthy M. Aminoclay: A functional layered material with multifaceted applications. *J. Mater. Chem. A* **1,** 6707 (2013).

48. Kumar R. K., Li M., Olof S. N., Patil A. J. & Mann S. Artificial cytoskeletal structures within enzymatically active bio-inorganic protocells. *Small* **9,** 357-362 (2013).

49. Li M., Huang X. & Mann S. Spontaneous growth and division in self-reproducing inorganic colloidosomes. *Small* **10,** 3291-3298 (2014).

50. Dora. Tang T. Y., van Swaay D., deMello A., Ross Anderson J. L. & Mann S. In vitro gene expression within membrane-free coacervate protocells. *Chem. Commun.* **51,** 11429-11432 (2015).

51. Bozzano G. & Dente M. Shape and terminal velocity of single bubble motion: A novel approach. *Comput. Chem. Eng.* **25,** 571-576 (2001).

52. Klein J., Stock J. & Vorlop K.-D. Pore size and properties of spherical ca-alginate biocatalysts. *European J. Appl. Microbiol. Biotechnol.* **18,** 86-91 (1983).

53. Patil A. J., Muthusamy E. & Mann S. Fabrication of functional protein-organoclay lamellar nanocomposites by biomolecule-induced assembly of exfoliated aminopropyl-functionalized magnesium phyllosilicates. *J. Mater. Chem.* **15,** 3838-3843 (2005).

54. Burkett S. L., Press A. & Mann S. Synthesis, characterization, and reactivity of layered inorganic−organic nanocomposites based on 2:1 trioctahedral phyllosilicates. *Chem. Mater.* **9,** 1071-1073 (1997).

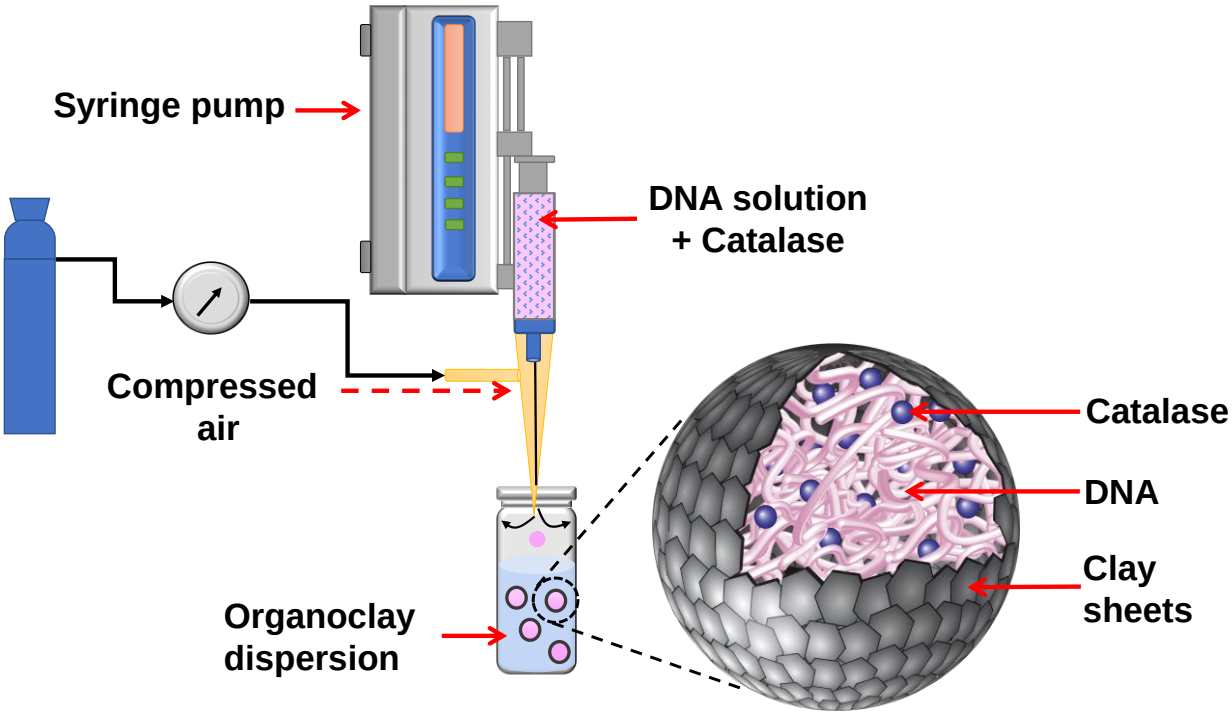

Figure 1| Fabrication of organoclay/DNA microcapsules. Schematic representation of the experimental procedure used for the fabrication of enzyme-powered organoclay/DNA microcapsules. An aqueous solution of polyanionic *ds*DNA and catalase was extruded through a syringe and sheared into microdroplets using a coaxial air jet.[52] Subsequent immersion of the droplets into an aqueous dispersion of exfoliated sheets of a cationic (zeta potential = +20 mV) aminopropyl-functionalised magnesium phyllosilicate (AMP) clay (approximate unit cell composition $[H_2N(CH_2)_3]_8Si_8Mg_6O_{16}(OH)_4$)[53, 54] gave rise to electrostatically induced self-assembly of an organoclay/DNA membrane specifically at the droplet surface and concomitant microcapsule formation. The semi-permeable membrane consisted of a matrix of electrostatically complexed DNA and organoclay sheets, and enclosed a concentrated solution of non-complexed DNA along with encapsulated catalase. In some experiments, glucose oxidase (GOx), alkaline phosphatase (ALP), calcium carbonate, silica or magnetic polymer microparticles, or other types of protocells (colloidosomes) were added to the DNA solution and co-encapsulated within the microcapsules using the above procedure.

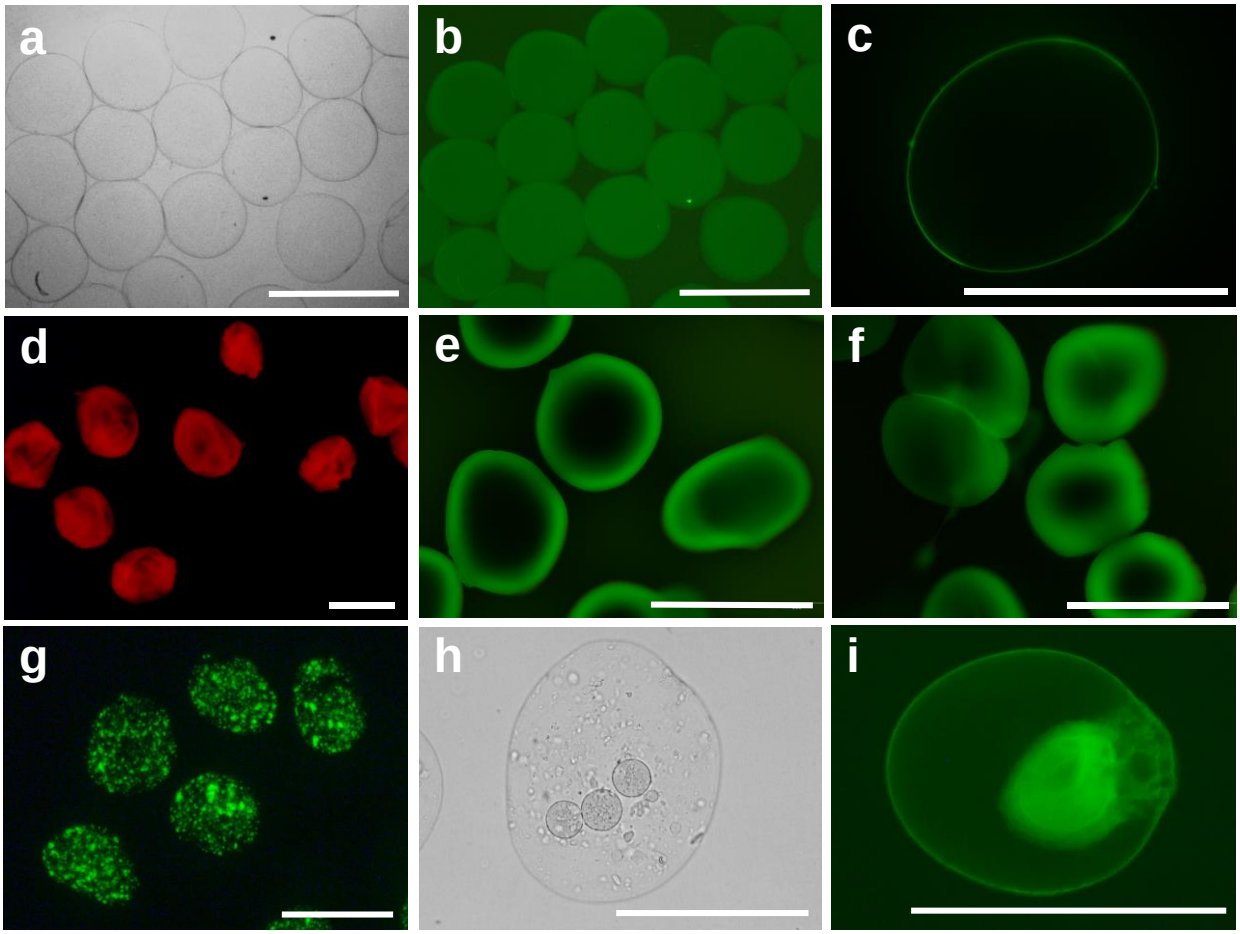

Figure 2| General properties of organoclay/DNA microcapsules. (a) Optical microscopy image of organoclay/DNA microcapsules produced at a shear rate of 10 µL/min. **(b)** Fluorescence microscopy image showing presence of encapsulated acridine orange-stained DNA within the aqueous lumen of organoclay/DNA microcapsules. **(c)** Fluorescence microscopy image of an individual microcapsule showing the pyranine-stained organoclay/DNA membrane with uniform thickness. **(d)** Fluorescence microscopy image showing osmotically induced shrinkage of organoclay/DNA microcapsules after addition of carboxymethyl dextran to the external medium. The image is recorded after 65 min. Fluorescence arises from the encapsulation of RITC-BSA within the capsules. Scale bar, 500 µm. **(e,f)** Fluorescence microscopy images showing time-dependent membrane permeation of acridine orange and progressive staining of free DNA within the lumen of organoclay/DNA microcapsules after 2 and 5 min, respectively. **(g)** Fluorescence microscopy image showing green fluorescent 3 µm-sized silica particles encapsulated within a population of organoclay/DNA microcapsules. **(h)** Optical microscopy image showing nested arrangement comprising the encapsulation of three colloidosomes within a single organoclay/DNA microcapsule. **(i)** Fluorescence microscopy image showing single organoclay/DNA microcapsule comprising a structured coacervate-like protamine/DNA interior. Condensation of free DNA molecules occurs by peptide uptake and electrostatically induced self-assembly within the micro-compartment. Images stained with acridine orange. All scale bars, 500 µm.

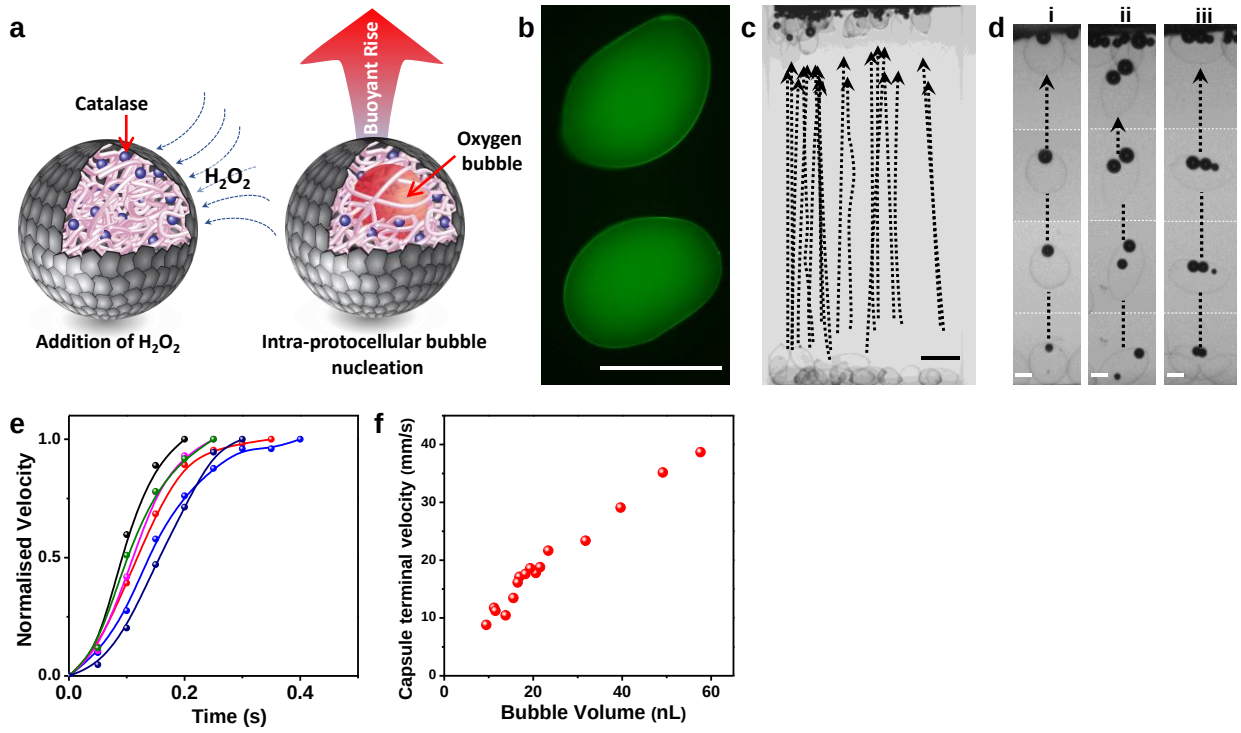

Figure 3| Buoyant motility in organoclay/DNA microcapsules. (a) Graphics showing diffusion of hydrogen peroxide into a catalase-containing organoclay/DNA microcapsule and subsequent nucleation, growth and entrapment of a single microbubble of oxygen. The bubble is stabilized by adsorption of encapsulated DNA and catalase molecules onto the gas/liquid interface, as well as by the resilience of the organoclay/DNA membrane. Growth of the microbubble by enzyme-mediated consumption of hydrogen peroxide allows the buoyant force to overcome the weight of the microcapsule and induce an upward trajectory of the microcapsule. **(b)** Fluorescence microscopy image showing green fluorescence associated with entrapment of FITC-labelled catalase within organoclay/DNA microcapsules; scale bar = 400 µm. **(c)** Composite optical microscopy image showing initial and final positions of 18 catalase-containing organoclay/DNA microcapsules before and after addition of hydrogen peroxide. The microcapsules are initially positioned at the bottom of the cuvette and rise to the air/water interface. The individual upward trajectories are shown as dashed lines for each microcapsule. See Supplementary video 1 for real time images of buoyancy-driven motility; scale bar = 800 µm. **(d)** Cropped optical microscopy images showing snapshots of three individual microcapsules containing one (**i**), two (**ii**) or three (**iii**) gas bubbles during their ascent to the air/water interface. The bubbles increase in size as they move upwards but do not coalesce. Bubble nucleation can also occur in transit (**iii**); scale bars = 200 µm. **(e)** Normalized velocity profiles for six individual catalase-containing organoclay/DNA microcapsules after addition of hydrogen peroxide showing attainment of terminal velocities within 0.4 s of motility. The spread of velocities is due to differences in the size of the entrapped oxygen bubbles. **(f)** Plot of microcapsule terminal velocities against entrapped microbubble volume showing linear correlation.

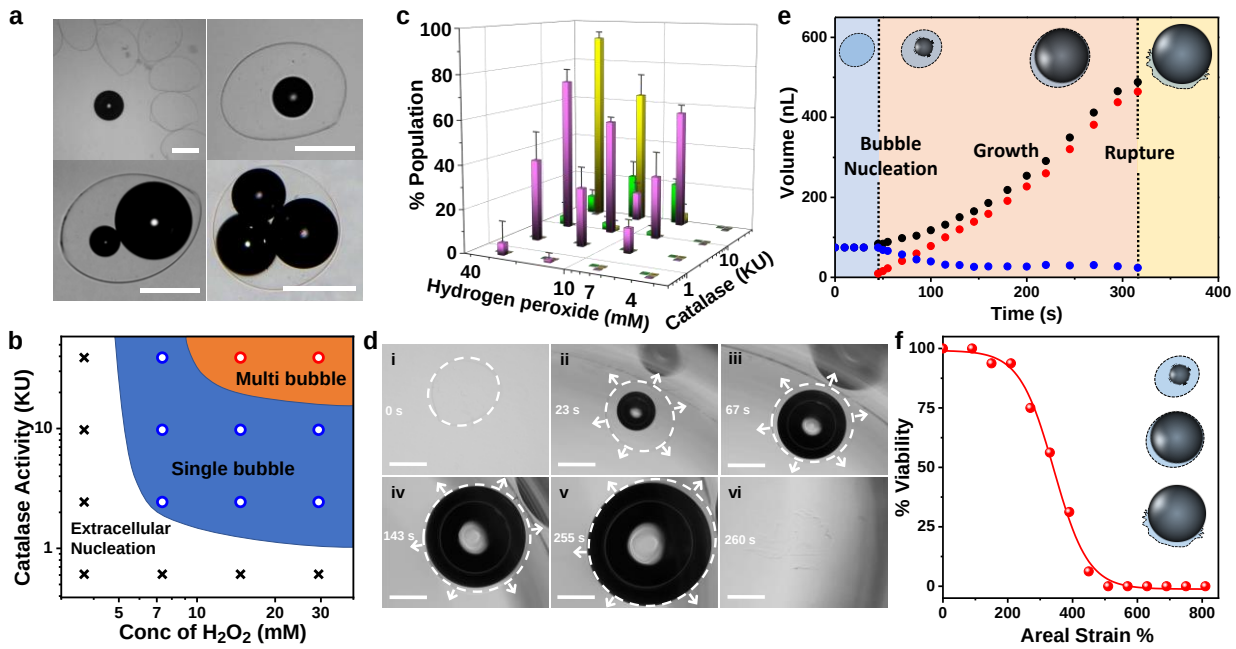

Figure 4| Nucleation and growth of oxygen microbubbles in organoclay/DNA microcapsules. (a) Optical bright field microscopy images showing catalase-containing organoclay/DNA microcapsules viewed under different enzyme/substrate conditions resulting in the absence of entrapped oxygen bubbles (top left), or nucleation of one, two or three discrete gas bubbles within protocells. Note the presence of the gas bubble outside the micro-compartments shown in the top left image, and absence of bubble coalescence in the other images; scale bars, 300 µm. **(b)** Plot showing three regimes of enzyme-mediated oxygen bubble production in organoclay/DNA microcapsules as a function of catalase and hydrogen peroxide concentrations. Each data point represents the dominant phenomenon observed in over 50 microcapsules from triplicate experiments; n > 10 microcapsules per experiment; n = 3 to 4 independent experiments. **(c)** Clustered 3D bar graphs showing percentage of microcapsule population containing 1 (magenta), 2 (green) or 3 or more (yellow) gas bubbles as a function of catalase and hydrogen peroxide concentrations. n > 10 microcapsules per experiment. n = 3 to 4 independent experiments. Error bars show standard error of mean. **(d)** Time sequence of optical microscopy images showing nucleation and growth of a single microbubble within an organoclay/DNA microcapsule. White dashed circles indicate the position of the low contrast microcapsule membrane before (**i**) and after bubble nucleation and growth (**ii-v**). Note the increasing volumetric strain and membrane rupture and collapse of the microcapsule shown in (**vi**); scale bars, 300 µm. **(e)** Plot showing changes of microcapsule volume (black), bubble volume (red) and entrapped aqueous phase volume (blue) for a single microcapsule as a function of internal bubble nucleation and growth. **(f)** Plot showing the viability of a population of sixteen catalase-containing organoclay/DNA microcapsules as a function of increasing areal strain generated by *in situ* bubble growth. Graphics in (**e**) and (**f**) depict associated changes in the volume of the entrapped gas bubble and encapsulated aqueous phase volume.

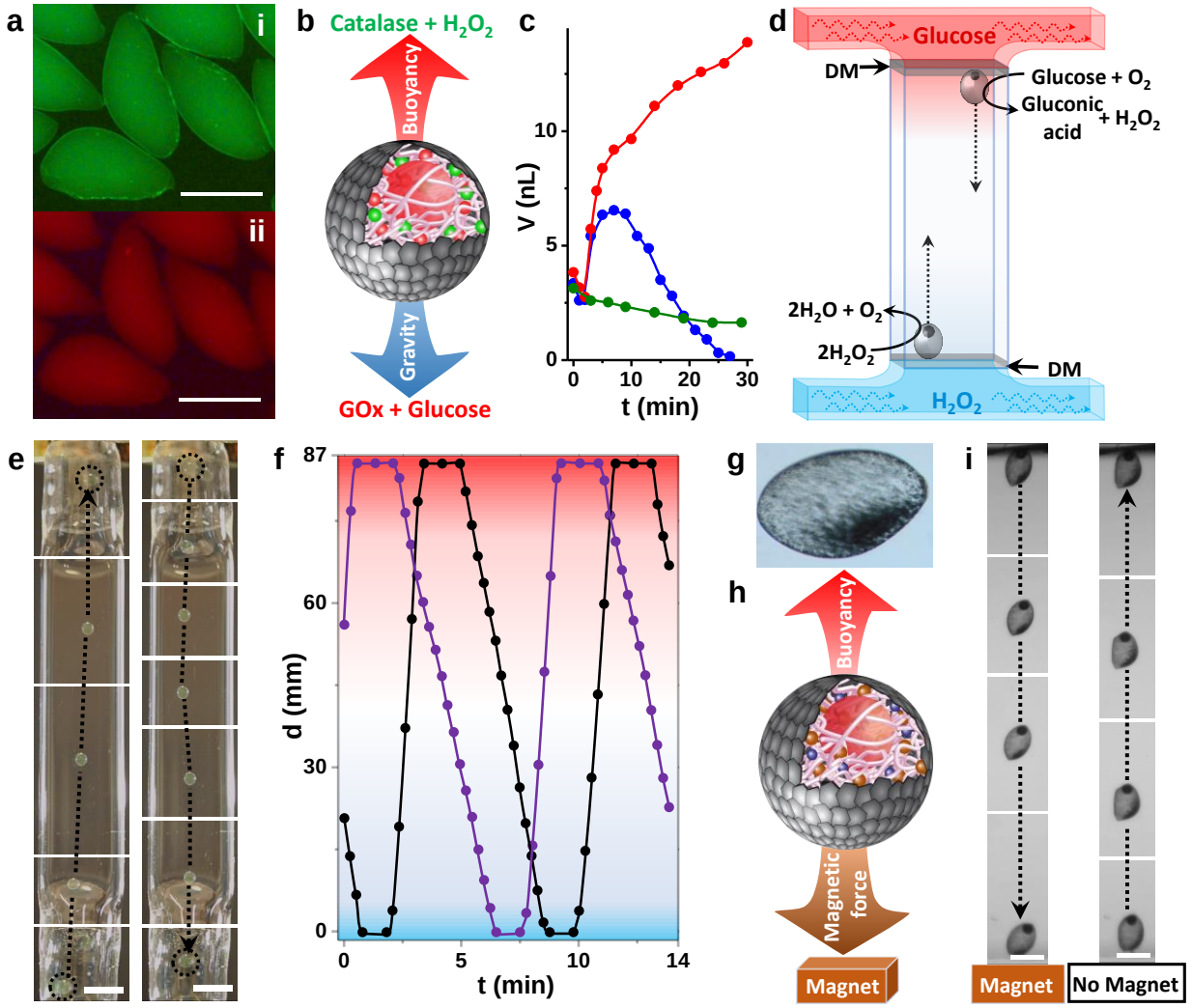

Figure 5| Oscillatory motion of organoclay/DNA microcapsules. **(a)** Green and red channel fluorescence microscopy images showing co-encapsulation of FITC-labelled catalase (i) and RITC-labelled GOx (ii) within organoclay/DNA microcapsules; scale bars = 500 µm. **(b)** Graphic illustrating competition between the buoyant force and gravity in an oxygen microbubble-containing microcapsule comprising catalase and GOx in the presence of externally added hydrogen peroxide and glucose. Consumption of the microbubble by GOx-mediated conversion of glucose to gluconic acid is used to decrease the buoyant force such that the capsule descends under gravity. **(c)** Plots showing time-dependent changes in volume (V/nL) of entrapped oxygen bubbles within buoyant catalase/GOx-containing organoclay/DNA microcapsules after addition of glucose (blue), sucrose (red) or water (green). The buoyant protocells are immobilized against a PDMS block that is suspended in an unstirred water column containing a hydrogen peroxide-rich bottom layer; glucose, sucrose or water solutions are injected close to the protocells trapped under the PDMS block. Complete consumption of the entrapped oxygen bubbles is observed on addition of glucose. No bubble decay occurs in the presence of sucrose; instead the bubbles grow as hydrogen peroxide diffuses into the upper layers of the water column due to density driven mixing in the presence of sucrose. Addition of water results in minimal change in bubble volume within an initial period of 30 min, indicating negligible passive mixing of the hydrogen peroxide layer. (**d**) Schematic representation of experimental set-up used to produce sustainable oscillatory movement of catalase/GOx-containing organoclay/DNA capsules. Aqueous solutions of hydrogen peroxide (1 %) and glucose (0.1 M) are flowed across the bottom and top of a water column containing enzyme-containing capsules to produce local gradients of the two substrates. The ends of the sample tube in contact with

the flowing solutions are covered in a dialysis membrane (**DM**; 10 kDa cut-off) to minimize hydrogen peroxide/glucose mixing whilst allowing slow diffusion of the substrates into the water column. The latter results in the formation of discrete zones that are rich in hydrogen peroxide or glucose at the bottom and top of the water column, respectively. As a result, oxygen bubble growth and consumption within the capsules occur at different ends of the water column to generate oscillatory buoyancy. **(e)** Time-lapse sequence of photographic images showing oscillatory vertical movement of a single catalase/GOx-containing organoclay/DNA capsule arising from spatiotemporal responses to antagonistic bubble generation and depletion at the bottom and top of the water column, respectively (see (**d**)). Images showing the catalase/hydrogen peroxide-mediated ascent of the capsule are recorded at 0, 15, 30, 45, 60 s (left column from bottom to top); images showing GOx/glucose-mediated descent are shown at 165, 195, 225, 255, 285, 315, 345 s (right column from top to bottom). Dashed circles highlight the capsule when partially obscured by the ends of the glass container; scale bars = 5 mm (see also supplementary video 4). **(f)** Plot showing time-dependent changes in vertical displacement (d/mm) for two organoclay/DNA capsules (purple and black traces) undergoing enzyme-mediated oscillatory movement. The water column is 85 mm in length and the protocell time periods are ca. 8 min. Blue and red shading indicate the localized concentration gradients in hydrogen peroxide and glucose, respectively. **(g)** Optical microscopy image showing magnetically responsive single organoclay/DNA microcapsule. Optically dark objects within the protocell correspond to encapsulated magnetic polymer microparticles; scale bar = 500 µm. **(h)** Graphic illustrating competition between magnetic and buoyant forces in a catalase-active protocell containing entrapped oxygen bubbles. **(i)** Time sequence of cropped optical microscopy images showing rapid changes in vertical displacement of a single catalase/magnetite-containing organoclay/DNA microcapsule undergoing oscillatory movement. Images showing the magnetically induced descent of the buoyant protocell are recorded at 0, 1.7, 2.0, and 2.3 s (left column from top to bottom); images showing buoyancy-induced ascent are recorded at 5.7, 6.3, 7.0. 8.0 s (right column from bottom to top). Scale bar = 500 µm. See also supplementary video 5.

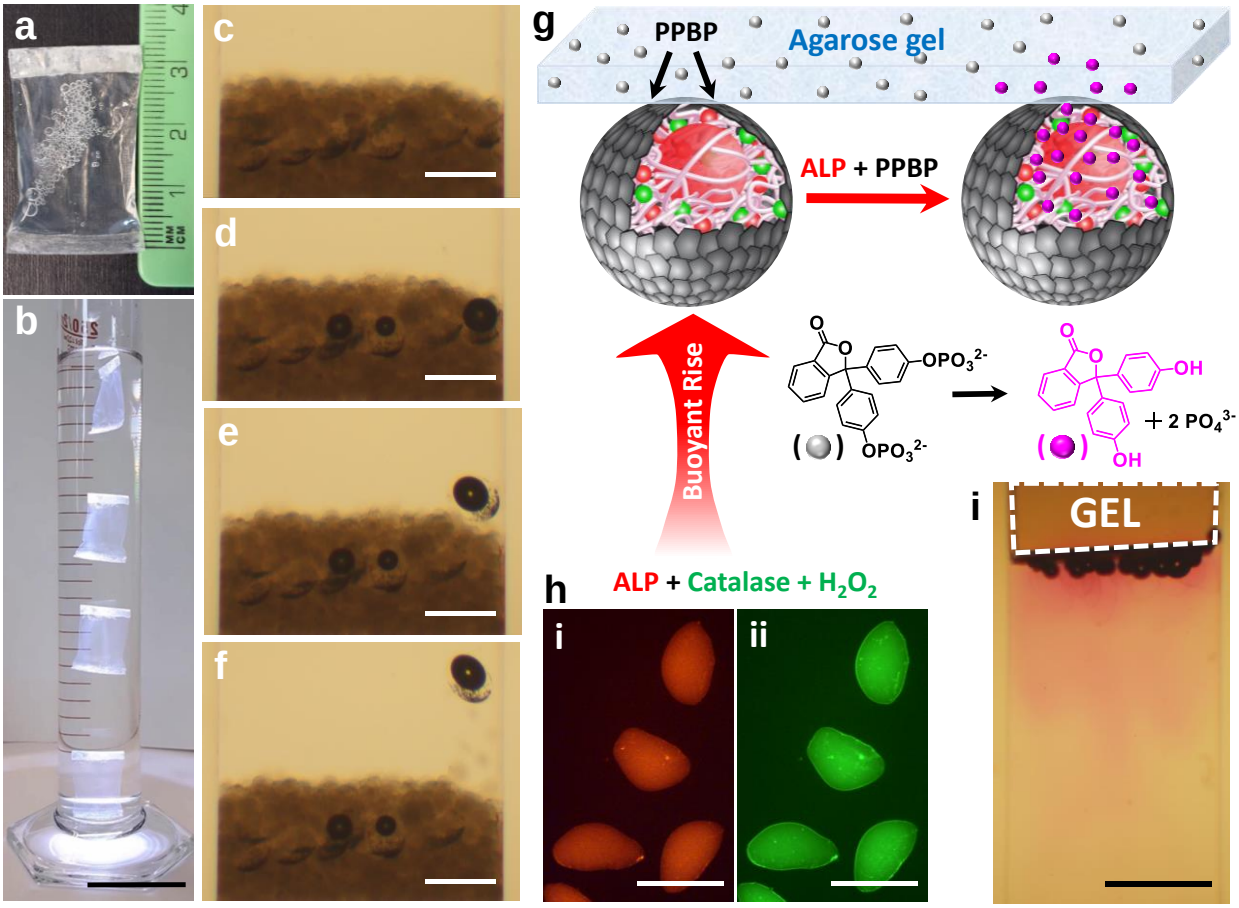

Figure 6|Properties of motile populations of organoclay/DNA microcapsules. (a) Photograph showing 3 cm-long sealed dialysis bag containing an aqueous dispersion of over 200 catalase-containing organoclay/DNA microcapsules. **(b)** Photographic image compiled from four separate photographs showing flotation of the dialysis bag viewed in (**a**) due to the buoyant force derived from catalase-mediated activity within the protocell population; scale bar = 4 mm. **(c-f)** Time sequence of optical microscopy images showing a mixed population of catalase-containing organoclay/DNA microcapsules and silica colloidosomes before **(c)**, and 100 (**d**) 107 **(e)** and 108 s **(f)** after addition of hydrogen peroxide. Addition of the substrate results in the nucleation of gas bubbles in the buried organoclay/DNA microcapsules **(d)**, followed by transit through the colloidosome matrix **(e)** and ejection into the solution as buoyant protocells **(f)**. Calcium carbonate microparticles were encapsulated in the microcapsules to increase the optical contrast against the background light scattering produced by the colloidosomes. Scale bars = 1 mm. **(g)** Scheme illustrating the use of catalase-mediated buoyancy of ALP-containing organoclay/DNA microcapsules as a mechanism for transferring the synthetic protocells from a passive to chemically active environment. The latter consists of a suspended agarose gel containing phenolphthalein bisphosphate (PPBP), which is dephosphorylated on arrival of the buoyant protocells, resulting in a pink coloration (phenolphthalein) within the microcapsules, gel and surrounding medium. **(h)** Red and green channel fluorescence microscopy images showing respectively co-encapsulation of RITC-labeled ALP (i) and FITC-labelled catalase (ii) within organoclay/DNA microcapsules; scale bars = 800 µm. **(i)** Optical microscopy image showing assembly of catalase/ALP-containing organoclay/DNA buoyant microcapsules (optically dark objects) 3-4 min after arrival at the surface of an agarose gel containing PPBP (white dashed box). Pink coloration in the adjacent aqueous phase corresponds to the ALP-mediated formation of phenolphthalein within the protocells and subsequent efflux into the surrounding solution. Scale bar = 2 mm.

Supplementary Information

Enzyme-powered motility in buoyant organoclay/DNA protocells

B.V.V.S. Pavan Kumar, Avinash J. Patil,* and Stephen Mann*

Centre for Protolife Research and Centre for Organized Matter Chemistry, School of Chemistry, University of Bristol, Bristol BS8 1TS, UK.
*e-mail: avinash.patil@bristol.ac.uk; s.mann@bristol.ac.uk

Contents

Supplementary videos

Supplementary video 1. Optical microscopy video showing buoyancy-induced motility in a 400 µL dispersion of catalase-containing organoclay/DNA microcapsules (26 KU/mL catalase; 2 mg/mL DNA) upon addition of 10 µL of hydrogen peroxide (294 mM). The video is shown in real-time.

Supplementary video 2. Fluorescence microscopy video showing growth of oxygen microbubbles within organoclay/DNA microcapsules containing catalase and FITC-BSA (2 mg/mL DNA; 39 KU/mL catalase; 0.2 mg/mL FITC-BSA). No apparent release of the FITC-BSA from the capsule interior is observed during the process of bubble growth and associated microcapsule expansion. The video is shown at x16 of real time. The total duration of the video is 2 min 56 s in real time.

Supplementary video 3. Optical microscopy video showing growth of oxygen bubbles within catalase-containing organoclay/DNA microcapsule (2 mg/mL DNA; 9.75 KU/mL catalase) upon addition of hydrogen peroxide (29.4 mM) and subsequent rupture of the microcapsule membrane releasing the entrapped bubble. The video is shown at different speeds (x4/x40 of real time) during different parts of the video and the speed at any given time is indicated at the top right corner. The total duration of the video is 9 min 35 s in real time.

Supplementary video 4. Digital camera video showing the oscillations of five organoclay/DNA capsules (3 mg/mL DNA, acridine orange-stained) containing catalase (52 KU/mL) and GOx (120 U/mL) within a specially designed apparatus for establishing substrate-rich zones on either end of the water column. Glucose (0.1 M) and hydrogen peroxide (1%) solutions are flowed across the top and bottom ends of the apparatus, respectively, to produce corresponding glucose or hydrogen peroxide-rich zones. The antagonistic activities of the two enzymes and their spatiotemporal dependence with regard to oxygen production (catalase) and consumption (GOx) result in oscillatory behavior. The video is shown at x30 of real time. The total duration of the video is 15 minutes in real time.

Supplementary video 5. Optical microscopy video showing the oscillatory movement of a single organoclay/DNA microcapsule containing catalase (39 KU/mL) and magnetic polymer microparticles (6 mg/mL) upon “on-off” exposure to an external magnetic field. In the “off” state, the buoyant force of the trapped bubble holds the microcapsule against the suspended PDMS block, whilst in the “on” state, the magnetic force is overrides the buoyant force resulting in the descent of the microcapsule to the bottom of the water column. The magnet is placed below the cuvette. The video is shown in real time for a total of 24 s.

Supplementary video 6. Digital camera video showing the flotation of a dialysis bag in a measuring cylinder containing 100 mL of water by the collective buoyant force harnessed by a large population of catalase-containing organoclay/DNA microcapsules (2 mg/mL DNA; 39 KU/mL catalase) upon addition of 400 µL of hydrogen peroxide (8.82 M). The video is shown at different

speeds (x2/x32 of real time) during different parts of the video and the speed at any given time is indicated at the top right corner. The total duration of the video is 7 min 40 s in real time.

Supplementary video 7. Optical microscopy video showing the segregation of a binary population of colloidosomes and catalase-containing organoclay/DNA microcapsules (2 mg/mL DNA; 39 KU/mL catalase) on addition of 20 µL of hydrogen peroxide (294 mM). The addition of the substrate results in the formation of oxygen bubbles preferentially in the buried organoclay/DNA microcapsules, followed by transit through the colloidosome matrix and ejection into the solution as buoyant protocells. Calcium carbonate microparticles are encapsulated in the microcapsules to increase the optical contrast against the background light scattering produced by the colloidosomes. The video is shown in x4 of real time speed. The total duration of the video is 76 s in real time.

Supplementary video 8. Optical microscopy video showing the collective motion of catalase/ALP-containing organoclay/DNA microcapsules (2 mg/mL DNA; 39 KU/mL catalase; 300 U/mL ALP) towards a suspended agarose gel containing phenolphthalein bisphosphate (PPBP). Accumulation of the microcapsules at the gel surface results in activation of ALP-mediated dephosphorylation of PPBP within the microcapsules to produce phenolphthalein (pink coloration). The video is shown at different speeds (x4/x40 of real time) during different parts of the video and the speed at any given time is indicated at the top right corner. The total duration of the video is 4 min 30 s in real time.

SI METHODS

Materials: All materials were used without further purification. Deoxyribonucleic acid sodium salt (DNA) from salmon testes (M_W ≈ 1300 kDa), magnesium chloride, 3-aminopropyltriethoxysilane, bovine serum albumin (BSA), rhodamine isothiocyanate (RITC), fluorescein isothiocyanate (FITC), phenolphthalein bisphosphate tetrasodium salt, acridine orange, catalase, agarose, sucrose, protamine sulfate salt from salmon (Grade X), glucose oxidase from *Aspergillus niger* (GOx, 120 U/mg), glucose and carboxymethyl-dextran sodium salt (M_W ≈ 10-20 kDa) were purchased from Sigma. Dialysis membrane (MWCO ≈ 12-14 kDa) was obtained from Medicell Membrane Ltd. Calf intestine alkaline phosphatase (31130 U/mL) was purchased from Calbiochem. Hydrogen peroxide (30 % w/v) was obtained from Fischer Scientific. FITC-tagged silica micro-particles and magnetic polymer microspheres (2.6 µm, COOH modified, 5% w/w) were bought from Bangs Laboratories Inc. Milli-Q water (18.2 MΩ·cm) was used in the preparation of all aqueous solutions.

Optical microscopy: Optical microscopy experiments were carried out on a Leica DMI 3000B optical microscope. Fluorescence imaging was performed using a Leica DFC 310FX set up, and dye molecules were excited by using specific filters with the following excitation (λ_{ex}) and emission wavelength (λ_{em}) cut offs: FITC and acridine orange, λ_{ex} = 450 - 490 nm and λ_{em} = 510 nm; RITC, λ_{ex} = 515 - 560 nm and λ_{em} = 580 nm.

Synthesis of magnesium phyllosilicate: Aminopropyl-functionalized magnesium phyllosilicate (AMP) clay was prepared according to a previously reported procedure.[1] Typically, AMP clay was prepared by dropwise addition of 3-aminopropyltriethoxysilane (1.3 mL, 5.85 mmol) to an ethanolic solution of magnesium chloride (0.84 g, 3.62 mmol). The white precipitate obtained after 5 minutes was stirred overnight and the precipitated product was collected by centrifugation, washed with ethanol for 3 times and dried at 40 ^{o}C.

Fluorescence labelling of enzymes: Fluorescein-isothiocyanate (FITC) was used to label catalase. Rhodamine-isothiocyanate (RITC) was used to label alkaline phosphatase (ALP) and glucose oxidase (GOx). In general, enzymes (10 mL, 4 mg/mL) were dissolved in sodium carbonate buffer (0.1 M, pH 8) and a dimethyl sulfoxide (DMSO) solution of FITC (200 µL, 2 mg/mL) or RITC (200 µL, 2 mg/mL) was added. The reaction mixtures were maintained at 4 °C for 12 h and then dialyzed against Millipore water for 3 days with regular water changes. The fluorescently labelled enzymes were recovered by lyophilization.

Fabrication of organoclay/DNA microcapsules: An exfoliated sol of AMP clay in water (5 mg/mL) was prepared by ultrasonication of an aqueous dispersion of the as-synthesized clay followed by membrane filtration (5 µm pore size). Spontaneous delamination of the as-synthesized clay occurred due to protonation-induced electrostatic repulsion between the pendent interlayer aminopropyl groups. A simple cost-effective co-axial extrusion device was fabricated for air-jet droplet generation. A syringe pump was used to dispense an aqueous solution of DNA (1-4 mg/mL) at flow rates of 10-50 µL/min through a syringe fitted with a hypodermic needle (30 gauge) and nozzle. A flow of air (2-5 L/min) was directed through a Tefzel tube (0.50 mm internal diameter, VICI, JR-T-082-M3) into the nozzle to generate a coaxial air jet around the needle to shear the extruded DNA into micro-droplets that produced organoclay/DNA microcapsules on entry into a freshly exfoliated AMP clay sol (5 mg/mL) placed below the nozzle. The microcapsules were isolated by ultracentrifugation (5000 rpm) and re-suspended in either 10 mM NaCl or 5 mM $MgCl_2$ solutions. Samples were stable for at least 5 days at room temperature.

Encapsulation of functional components within the organoclay/DNA microcapsules was achieved by addition of dyes, proteins, enzymes, particle suspensions or colloidosome dispersions to the DNA aqueous solution prior to droplet formation. The following samples were prepared by interfacial stabilization of DNA-containing droplets (2 mg/mL) in the presence of exfoliated AMP (5 mg/mL): (i) dye-stained capsules (acridine orange (10 mM); (ii) protein-containing capsules (RITC-BSA/FITC-BSA (0.2 mg/mL), or ferritin (0.5 mg/mL)); (iii) particle-containing capsules (magnetic polymer microparticles, (5 mg/mL), fluorescent silica particles (5 mg/mL) or calcium carbonate microparticles (40 mg/mL), (iv) colloidosome-containing capsules (7.04×10^4 colloidosomes/mL) and (v) enzyme-containing capsules (catalase (52, 39, 9.75, 2.44 or 0.61 KU/mL), fluorescein isothiocyanate-labelled catalase (0.8 or 0.4 mg/mL), alkaline phosphatase, ALP (1 U/mL), RITC-ALP (0.3 mg/mL), glucose oxidase (GOx, (24 U/mL) or RITC-GOx (0.5 mg/mL)).

Staining of the organoclay/DNA microcapsule membrane was undertaken using the anionic dye pyranine; samples were exposed to an aqueous solution of the dye, and then the dye solution exchanged with water to remove any unbound dye molecules. Microcapsules were imaged by

fluorescence optical microscopy and the membrane thickness calculated from the full width at half maximum (FWHM) of the fluorescence intensity profiles.

Membrane permeability and microcapsule deformability studies: 100 µL of glucose (0.5 M) or carboxymethyldextran (2.5 mg/mL) was added to 100 µL of a dispersion of organoclay/DNA microcapsules and osmotically-induced changes in shape of the microcompartments recorded by optical microscopy. Membrane diffusion and uptake of acridine orange was monitored by time-dependent fluorescence microscopy imaging of aqueous dispersions of organoclay/DNA microcapsules (100 µL) after addition of 1 µL of acridine orange (10 mM) (excitation 450-490 nm, emission cut-off 510 nm). Similar experiments were undertaken in the presence of RITC-BSA (100 µL, 0.4 mg/mL), pyranine (100 µL, 0.2 mM) and rhodamine 6G (100 µL, 0.1 mM) to assess the uptake/exclusion of the organoclay/DNA microcapsules to proteins and dye molecules. To study the deformability of the organoclay/DNA microcapsules, 50 µL of a dispersion of the microcapsules was placed on a microscope glass slide and compressed by placing a coverslip over the sample. The coverslip was then removed to determine the reversibility of the deformation process. Deformation of the microcapsules was followed using an optical microscope.

DNA/protamine coacervation in organoclay/DNA microcapsules: 10 µL of protamine sulfate (10 mg/mL) was added to a 100 µL dispersion of acridine orange-stained organoclay/DNA microcapsules (2 mg/mL DNA, 10 mM acridine orange). Condensation of the DNA induced by protamine sulfate was followed using a fluorescence microscope, and was completed typically within 10-15 minutes.

Alkaline phosphatase (ALP) activity in organoclay/DNA microcapsules: 40 µL of microcapsules (2 mg/mL DNA) containing ALP (1 U/mL) were added to 460 µL of water (pH 9.8, adjusted by 1M NaOH) in a quartz cuvette (path length 1 cm) and placed in a UV/Vis spectrophotometer (Perkin Elmer Lambda 25). To avoid scattering effects, the microcapsules were allowed to sediment so that the optical beam passed only through a clear aqueous medium. Subsequently, various amounts of *p*-nitrophenylphosphate (0.25 M) were added to the cuvette and the production of *p*-nitrophenol associated with the encapsulated ALP was monitored at room temperature by changes in absorption at 410 nm. Assays on free ALP (40 µL, 1 U/mL) in the absence of organoclay/DNA microcapsules were undertaken using a similar protocol in unbuffered (pH 9.8, adjusted by 1M NaOH) and buffered media (1.0 M diethanolamine, 0.5 mM $MgCl_2$, pH 9.8). Assays were performed in triplicate, and the Michaelis-Menten kinetic parameters determined from fits to the dependence of average initial reaction rates (v_o) on substrate concentration (S) using Origin 9.0 software. The equation used for fitting was:

$$\vartheta o = \frac{Vmax[S]}{Km + [S]}$$

where, V_{max} is the maximum reaction velocity and K_m the Michaelis constant. k_{cat} was determined as V_{max} / [E_t], where E_t corresponds to total enzyme concentration. The catalytic efficiency was given by k_{cat}/K_m.

Fabrication of buoyant organoclay/DNA microcapsules: Oxygen bubble generation was induced by addition of hydrogen peroxide to a dispersion of catalase-containing organoclay/DNA microcapsules. DNA solutions containing catalase at concentrations of 39, 9.75, 2.44 or 0.61 KU/mL enzyme were prepared by mixing appropriate amounts of a catalase stock solution (65 KU/mL) with 100 µL of aqueous DNA (5, 10 or 20 mg/mL) and making up the volume to 500 µL with water. Enzyme-containing droplets were then produced by air-jet coaxial extrusion and stabilized as organoclay/DNA microcapsules by immersion into an exfoliated AMP sol. Controlled numbers of selected catalase-containing capsules were transferred individually or as concentrated dispersions to quartz cuvettes or well plates using a glass pipette prior to addition of hydrogen peroxide. Typically, a catalase concentration of 39 KU/mL was used to produce buoyant microcapsules in the presence of 29.4 mM of aqueous hydrogen peroxide.

Buoyancy-induced motility in catalase-containing organoclay/DNA protocells: To study the vertical (*z* direction) motion of the buoyant organoclay/DNA microcapsules, a Zeiss Axioskop microscope (1.25x objective lens) was aligned side-on to a quartz cuvette to switch the viewing plane from *xy* to *yz/xz*. An aqueous dispersion of catalase-containing microcapsules (*ca*. 100 µL; 2 mg/mL DNA; 9.75 or 39 KU/mL catalase) was pipetted into a quartz cuvette containing *ca*. 300 µL of a dilute dispersion of AMP clay (0.5 mg/mL), and the organoclay/DNA capsules allowed to sink to the bottom of the sample holder. In some experiments, the microcapsules were pretreated with protamine sulfate solution (0.025 mg/mL) for 10-15 minutes to condense the encapsulated DNA, and thereby improve the image contrast. The AMP clay sol was used to minimize adsorption onto the walls of the cuvette. The cuvette was cleaned in piranha solution every few experiments to avoid nucleation of oxygen bubbles on the walls of the sample container. A small self-supporting block of PDMS (*ca.* 4 x 3 x 3 mm) was mounted across part of the cuvette channel (width, 4 mm) approximately 8 mm from the bottom such that it served as a suspended platform for trapping and imaging the buoyant protocells after their vertical displacement in the presence of hydrogen peroxide. The PDMS block did not extend completely across the width of the cuvette so that local injection of hydrogen peroxide (10 µL, 294 mM) into the solution could be undertaken above or below the platform. Vertical motion of the buoyant microcapsules was recorded by optical microscopy. See Supplementary Fig. 19 for a schematic representation of the experimental set-up.

Gas bubble nucleation and growth: ***Nucleation:*** Approximately 15-25 catalase-containing organoclay/DNA microcapsules prepared as above with a range of enzyme and DNA concentrations were dispersed in 100 µL of water using a glass pipette, and then placed in each well of a well-plate. 100 µL of hydrogen peroxide (3.7, 7.3, 14.7 or 29.4 mM) were then added to each well. The number of oxygen bubble nucleation events occurring per microcapsule was monitored using optical microscopy. ***Growth****:* Using the above procedure, growth of oxygen bubbles within catalase-containing organoclay/DNA microcapsules was monitored by optical microscopy recordings of time-dependent changes in the volume of the bubbles, along with associated changes in the volume of the encapsulated liquid phase and volume of the microcapsule. Image analysis was carried out using Image J, assuming that the bubbles were prolate ellipsoids with their long axis in the plane of the image. The net displacement of the

microcapsules in the vertical (*z*) direction across two successive frames in the video was used to calculate the instantaneous velocity. Fluorescein isothiocyanate-labelled catalase (0.8 mg/mL) and FITC-BSA (0.2 mg/mL) were co-encapsulated into the enzyme-containing microcapsules (2mg/mL DNA; 39 KU/mL catalase), and fluorescence microscopy used to monitor the displacement of encapsulated guest molecules during bubble growth. The effect of bubble overgrowth and concomitant bursting of the microcapsule was undertaken using optical microscopy to monitor single micro-compartments (2 mg/mL DNA; 9.75 KU/mL catalase) that were dispersed using a glass pipette into 100 µL of water in a well plate, and exposed to 100 µL of hydrogen peroxide (58.8 mM). Image analysis was used to determine the areal strain experienced by the microcapsules at the bubble-induced breaking point. The percentage areal strain was given by [change in surface area]/[initial surface area] x 100.

Enzyme-powered oscillatory movement in organoclay/DNA capsules: A series of up/down motions was induced in the buoyant organoclay/DNA capsules by spatially separating oxygen bubble production and depletion associated with catalase or glucose oxidase (GOx) activity, respectively. For this, a specially constructed glass apparatus (Supplementary Fig. 15) consisting of a central column with a middle rectangular cross section attached via rounded ground glass joints to T-junctions on either end, was employed for producing oscillatory vertical movement of catalase/GOx-containing organoclay/DNA capsules. A glucose solution (0.1 M) was supplied through silicone tubing to the T-junction at the top of the column. Similarly, a hydrogen peroxide solution (294 mM) was supplied through silicone tubing to the T-junction at the bottom. The solutions at either end were separated from the central column by a dialysis membrane (10 kDa cut-off) placed in the ground-glass junctions, which were then sealed with parafilm. The organoclay/DNA capsules (3 mg/mL) containing catalase (52 KU/mL) and GOx (120 U/mL) were allowed to sediment in the water column. The capsules were pretreated with protamine solution (0.5 mg/mL) to increase contrast and stability. The supply of hydrogen peroxide at the bottom end triggered buoyancy followed by sustainable oscillations as the capsules reached the upper end and became depleted in oxygen by glucose/GOx activity. Movement of the capsules was followed using a digital camera (Canon EOS 500D). Millimeter-sized acridine-stained capsules were used to aid visual imaging of the oscillations. Image analysis was carried out using Image J to study the periodicity of oscillations, residence times, and the speeds of ascent and descent of the capsules.

Magnetic field-mediated buoyancy oscillations*:* A single organoclay/DNA microcapsule (2 mg/mL DNA) containing catalase (39 KU/mL) and magnetic polymer microparticles (6 mg/mL) was placed in a cuvette filled with 400 µL of a dilute dispersion of AMP clay and containing a suspended PDMS block. 1 µL of hydrogen peroxide (73.5 mM) was locally injected near to the microcapsule to induce buoyancy. The vertical displacement of the microcapsule was then controlled magnetically by placing or removing a magnet under the cuvette to oppose the buoyant force. The oscillatory trajectories of the microcapsules were recorded using optical microscopy.

Properties of motile organoclay/DNA protocell populations. ***Flotation of macroscopic objects:*** An aqueous dispersion of more than 200 catalase-containing organoclay/DNA microcapsules (2

mg/mL DNA, 39 KU/mL catalase) was pipetted into a dialysis bag of length 3-4 cm, and the ends of the bag sealed with superglue. The dialysis bag was placed in a measuring cylinder containing 100 mL of water, and 400 µL of hydrogen peroxide (8.82 M) was added. Flotation of the dialysis bag by the coordinated motion of the microcapsules was recorded using a camera (Canon EOS 500D*).* ***Segregation of mixed protocell communities:*** Organoclay/DNA microcapsules (2 mg/mL DNA) containing catalase (39 KU/mL) and calcium carbonate microspheres (40 mg/mL) were sedimented amongst a larger population of silica colloidosomes[30,31] in a cuvette by sequentially adding 100 µL of an aqueous dispersion of colloidosomes, 50 µL of a dispersion of microcapsules, and an additional 100 µL of the colloidosomes to *ca.* 300 µL of water. The dispersions were allowed to stand for 2-3 min after each addition. The calcium carbonate microparticles were included in the microcapsules to increase the optical contrast against the background light scattering produced by the colloidosomes. 20 µL of hydrogen peroxide (294 mM) was added to the cuvette to trigger the buoyancy-induced motility of the organoclay/DNA microcapsules embedded amongst the colloidosomes, and the motion recorded using an optical microscope. ***Transfer between different chemical environments:*** Organoclay/DNA microcapsules (2 mg/mL DNA) containing ALP (300 U/mL) and catalase (39 KU/mL) were placed at the bottom of a cuvette filled with 600 µL of a dilute dispersion of AMP clay in carbonate buffer (25 mM, pH 9). Instead of the suspended PDMS platform, the cuvette contained a self-supporting block of agarose gel (2% agarose) that was formed in the presence of the ALP-substrate phenolphthalein bisphosphate (8.82 mM) and positioned *ca*. 18 mm above the microcapsules. 20 µL of hydrogen peroxide (294 mM) were injected below the agarose gel platform to trigger motion of the microcapsules upwards towards the substrate-loaded gel. Subsequent ALP-mediated dephosphorylation and production of phenolphthalein was followed by optical microscopy

References:

1. Burkett S. L., Press A. & Mann S. Synthesis, Characterization, and Reactivity of Layered Inorganic−Organic Nanocomposites Based on 2:1 Trioctahedral Phyllosilicates. *Chem. Mater.* **9,** 1071-1073 (1997).

SI FIGURES

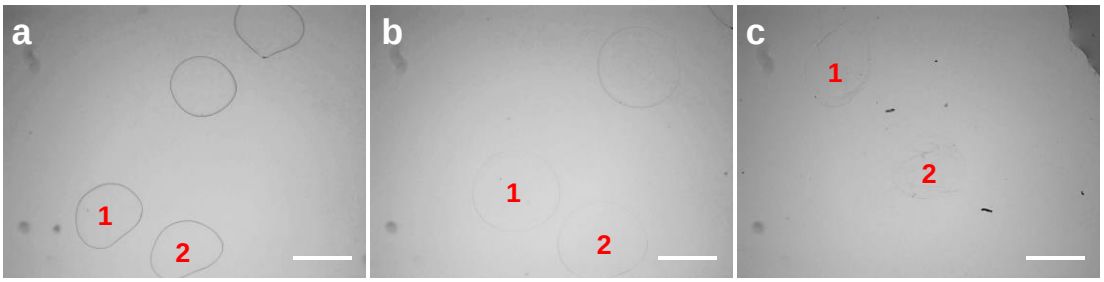

Figure 1. (**a-c**) Sequence of optical microscopy images of organoclay/DNA microcapsules demonstrating their deformability under compression. The labeled microcapsules (**1, 2**) are shown before compression (**a**), upon compression with a coverslip showing deformation (**b**), and after release of the compression force upon removal of the coverslip (**c**). All scale bars, 500 µm.

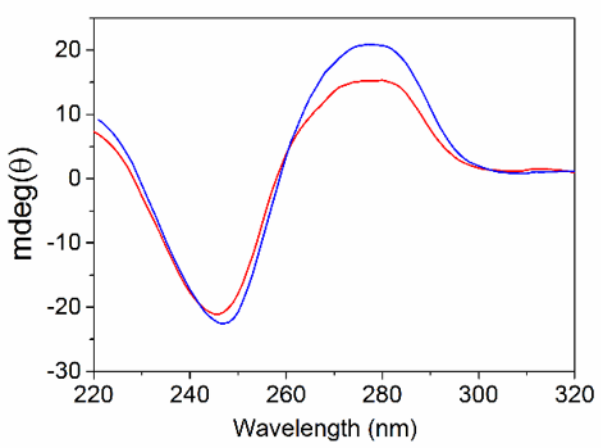

Figure 2. Circular dichroism spectra of free DNA (blue line) and organoclay/DNA microcapsules (red line) showing similar spectra indicating retention of the helical structure of *ds*DNA in the microcapsules.

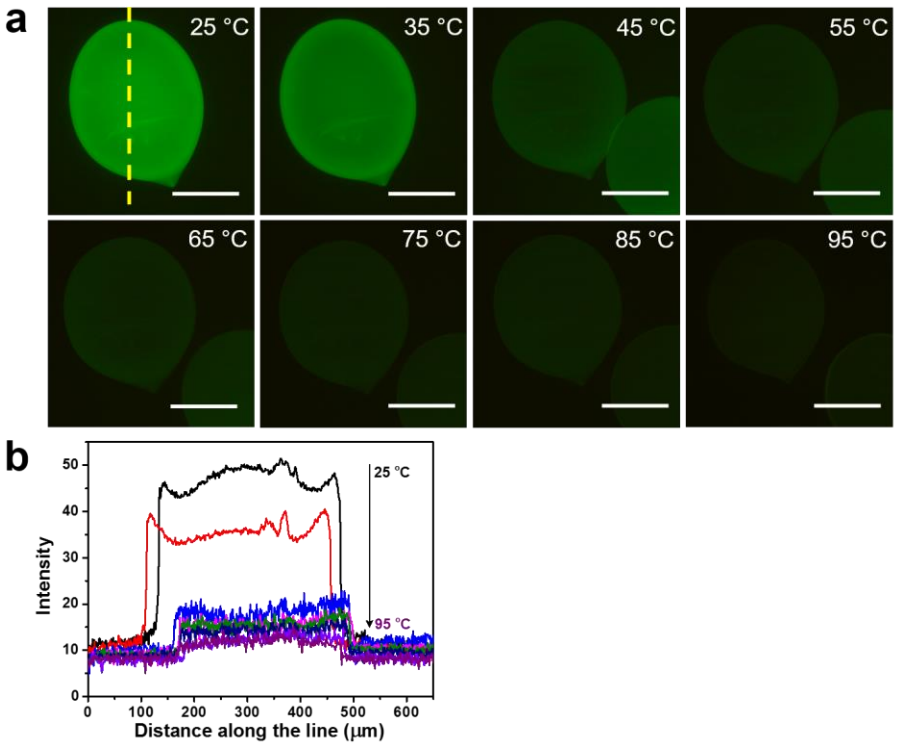

Figure 3. (**a**) Sequence of fluorescence microscopy images of acridine-orange stained organoclay/DNA microcapsules showing melting of free *ds*DNA in the microcapsule interior with increase in temperature (25-95°C) as indicated by the concomitant loss of fluorescence intensity. All scale bars, 200 µm. (**b**) Corresponding fluorescence-intensity line profiles at different temperatures showing maximum decrease in intensity between 35-45 °C corresponding to the melting temperature.

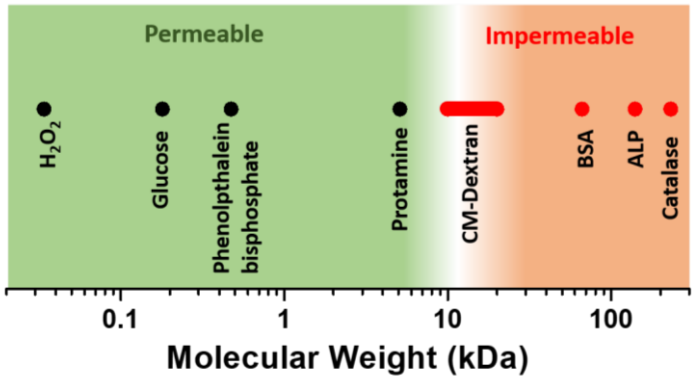

Figure 4. Summary plot showing dependence of solute molecular weight on the membrane permeability of organoclay/DNA microcapsules. Permeable (green region) and impermeable (orange region) solutes are shown. The molecular cut-off associated with passive transport across the organoclay/DNA membrane is shown (white diffuse region).

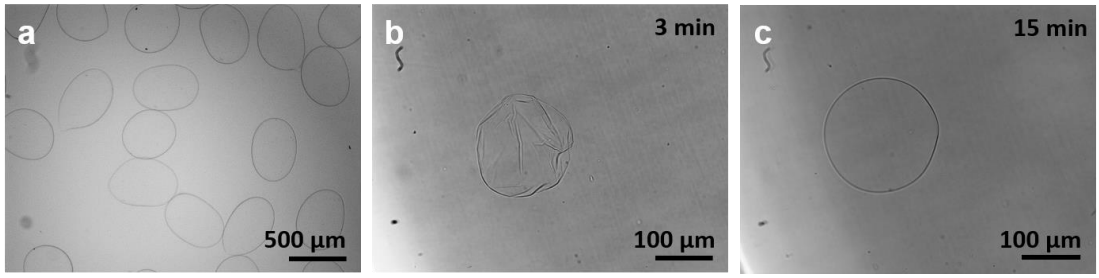

Figure 5. Sequence of optical microscopy images showing semi-permeable organoclay/DNA microcapsules undergoing temporary osmotic pressure-induced shrinkage on addition of 100 µL of 0.5 M glucose to a 100 µL aqueous dispersion. The initial circular/ellipsoidal shape of the microcapsules **(a)** partially collapses on addition of glucose **(b)**, before reverting back to the original morphology on equilibration of glucose levels across the organoclay/DNA membrane **(c)**.

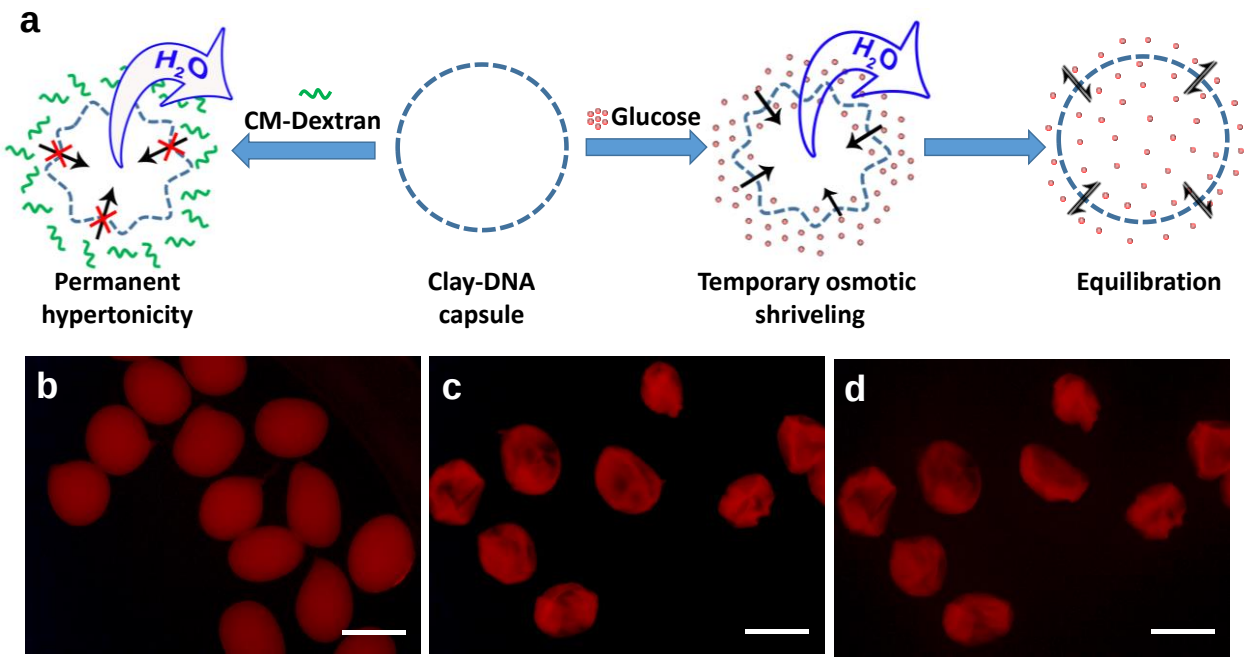

Figure 6. (**a**) Schematic showing osmotically induced changes in the shape of semi-permeable organoclay/DNA microcapsules on addition of different solutes to the external medium. Addition of small solutes such as glucose (0.25 M) establishes a temporary hypertonicity causing transient shrinkage of the microcapsules and subsequent relaxation to the original shape on equilibration of the solute levels across the membrane. Alternatively, addition of long chain polymers such as carboxymethyl dextran (10-20 kDa, 2.5 mg/mL) causes permanent shrinkage of the microcapsules due to their membrane impermeability. (**b-d**) Fluorescence microcopy images showing RITC-BSA-containing organoclay/DNA microcapsules before (**b**), after 65 minutes (**c**), and after 180 minutes (**d**) of addition of carboxymethyl dextran to the external medium. All scale bars, 500 µm.

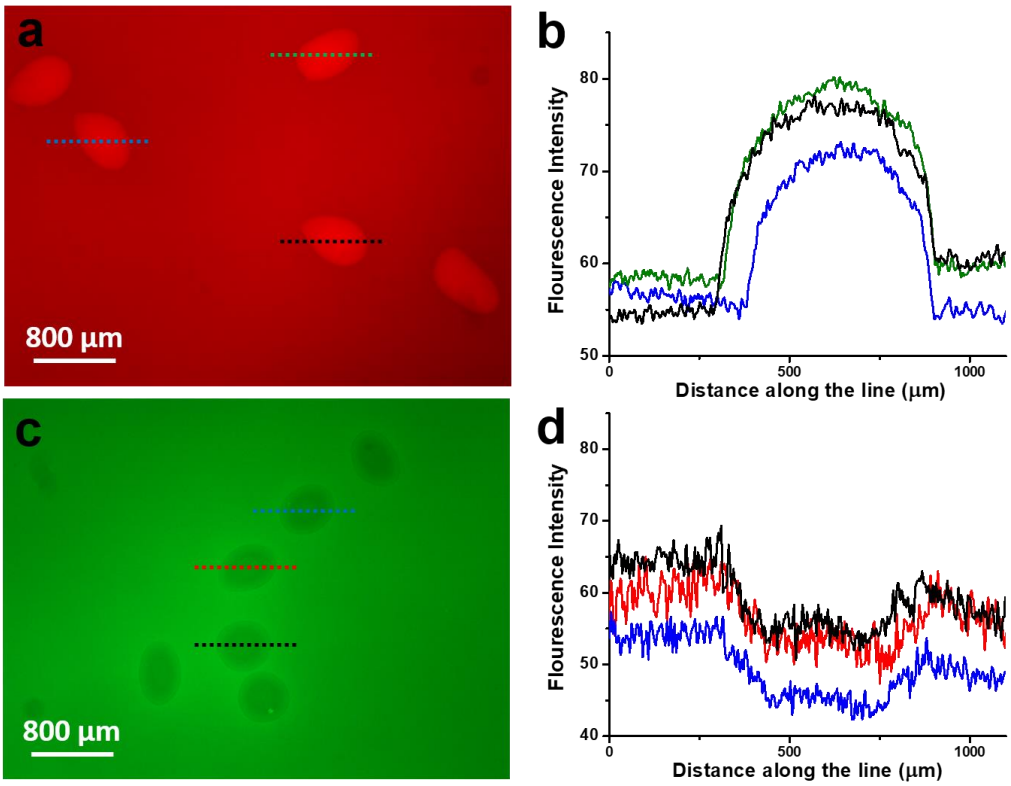

Figure 7. Dye uptake/exclusion studies. Fluorescence microscopy images of organoclay/DNA microcapsules demonstrating the uptake of rhodamine 6G within 10 min (a) and partial exclusion of pyranine (c). (b,d) Corresponding fluorescence intensity line profiles of selected microcapsules shown in the fluorescence images.

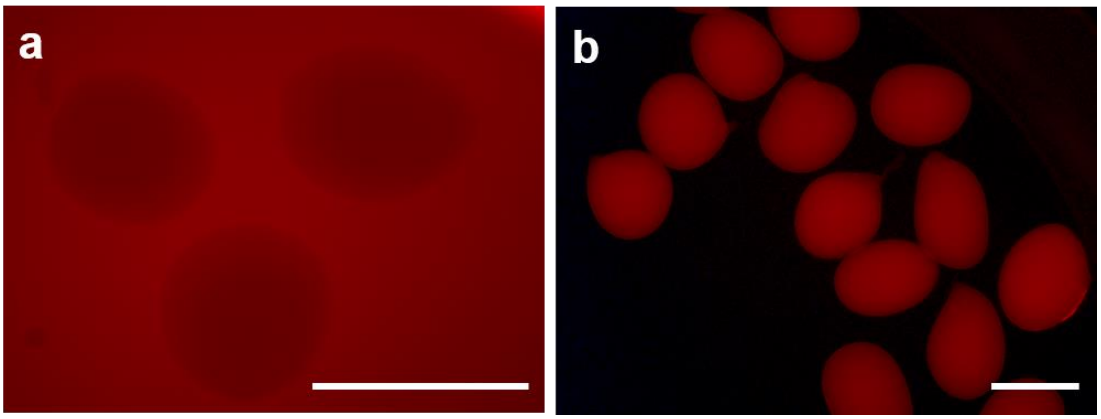

Figure 8. Fluorescence microscopy images showing (**a**) absence of uptake of rhodamine-labelled bovine serum albumin (RITC-BSA) into organoclay/DNA microcapsules after 30 min of exposure, and (**b**) successful encapsulation of RITC-BSA in the microcapsules; all scale bars, 500 µm.

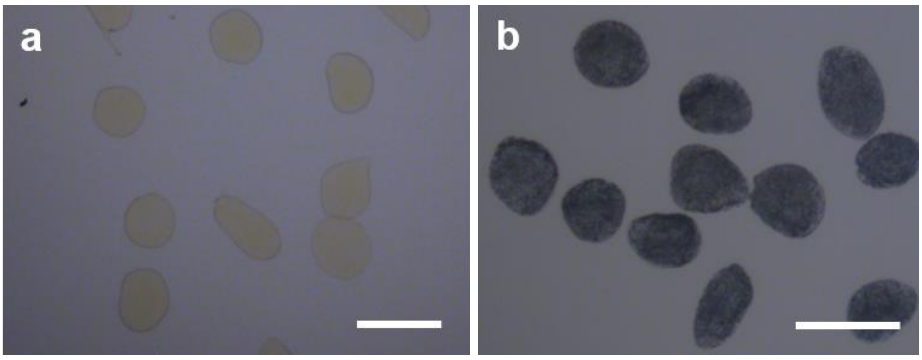

Figure 9. Optical microscopy images showing successful encapsulation of ferritin **(a)** and magnetic microparticles **(b)** within organoclay/DNA microcapsules. All scale bars, 500 µm.

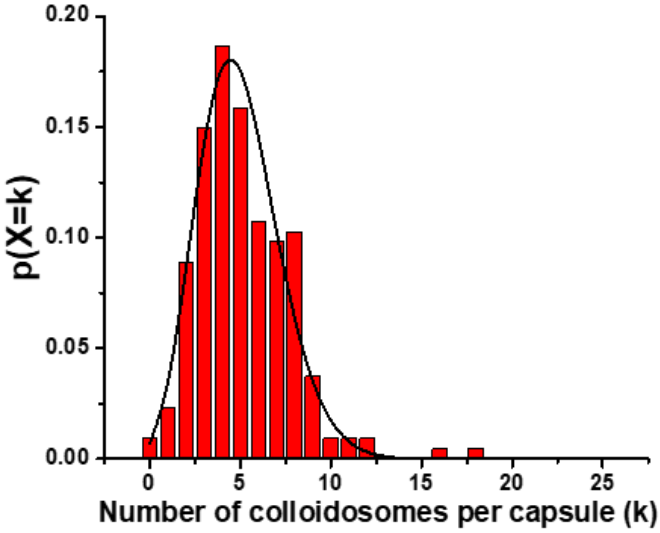

Figure 10. Plot showing the encapsulation distribution of cross-linked silica colloidosomes in individual organoclay/DNA microcapsules. The histogram and black line represent experimental data and the theoretical Poisson distribution, respectively. The colloidosome number density in the DNA solution used for microcapsule preparation was 7.04 x 10^4 colloidosomes/mL with a theoretical mean value of 4.96 colloidosomes per organoclay/DNA microcapsule. Approximately 215 microcapsules were analysed and 1102 colloidosomes counted resulting in a mean value of 5.15 colloidosomes per organoclay/DNA microcapsule.

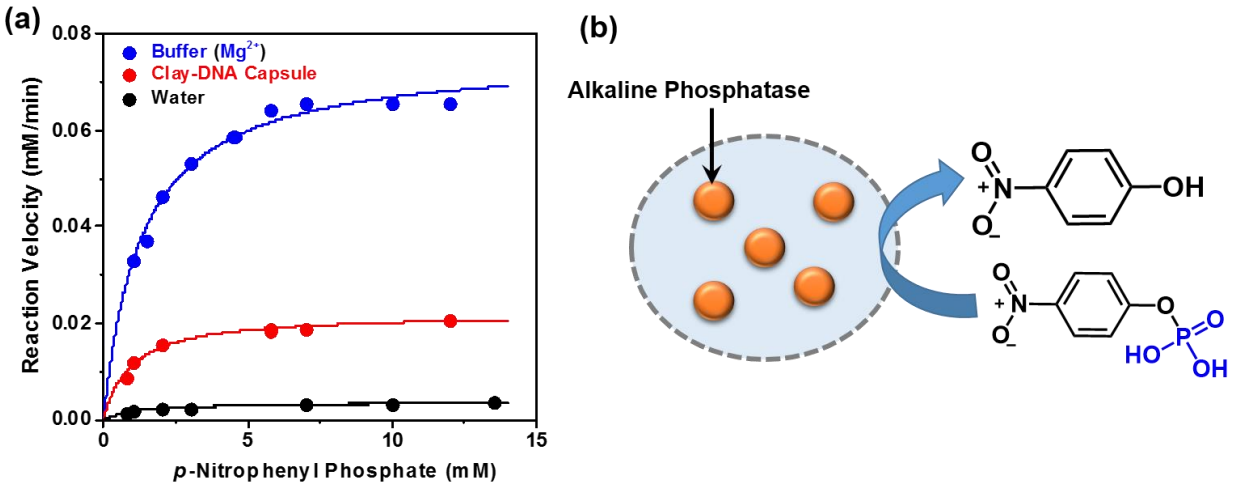

(c)

Sample	V_{max} (mM min^{-1})	K_m (mM)	k_{cat} (s^{-1})	k_{cat}/K_m ($M^{-1}s^{-1}$)
ALP in Water, pH 9.8	0.0037	1.20	1.07	0.82 x 10^3
ALP in Diethanolamine $MgCl_2$ Buffer, pH 9.8	0.075	1.32	21.88	1.67 x 10^4
ALP in Clay-DNA microcapsules, pH 9.8	0.022	0.94	6.41	6.808 x 10^3

Figure 11. (**a**) Enzyme-mediated dephosphorylation of *p*-nitrophenyl phosphate by alkaline phosphatase (ALP) in Mg^{2+}-containing buffer (blue), in water (black) or encapsulated within organoclay/DNA microcapsules. (**b**) Schematic representation of the ALP-mediated dephosphorylation reaction within the microcapsules showing release of nitrophenol, which is monitored by UV-vis spectroscopy. (**c**) Table showing kinetic parameters for enzymatic reactions undertaken in water, buffered solution or within the organoclay/DNA micro-compartments.

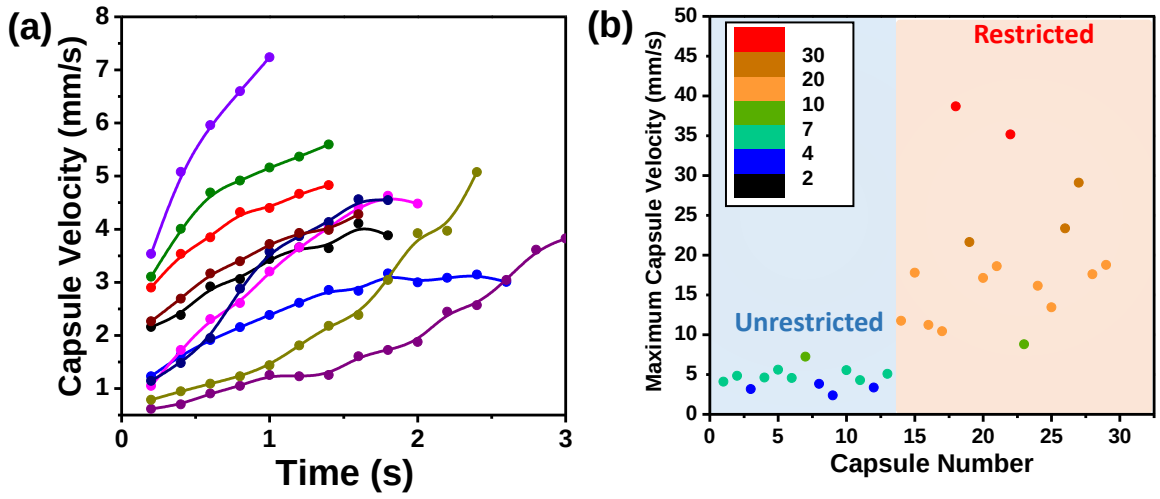

Figure 12. (**a**) Velocity profiles for ten physically unrestricted catalase-containing organoclay/DNA microcapsules showing accelerating protocells but no attainment of a terminal velocity. Velocities of less than 10 mm s^{-1} are generally observed over a 3 s transit time from the bottom to the top of the cuvette. Individual profiles differ due to differences in the rate of expansion of the entrapped gas bubbles in different protocells. Cross interference due to collision of the moving microcapsules gives rise to small deviations in the trajectories of some of the motile microcapsules. (**b**) A color-mapped scatter plot showing the spread of maximum velocity values determined for unrestricted microcapsules and physically restricted organoclay/DNA microcapsules. Gas bubbles in the restricted microcapsules grow to a maximum size before release into the water column and thus attain a terminal velocity of 10-40 mm s^{-1} during transit.

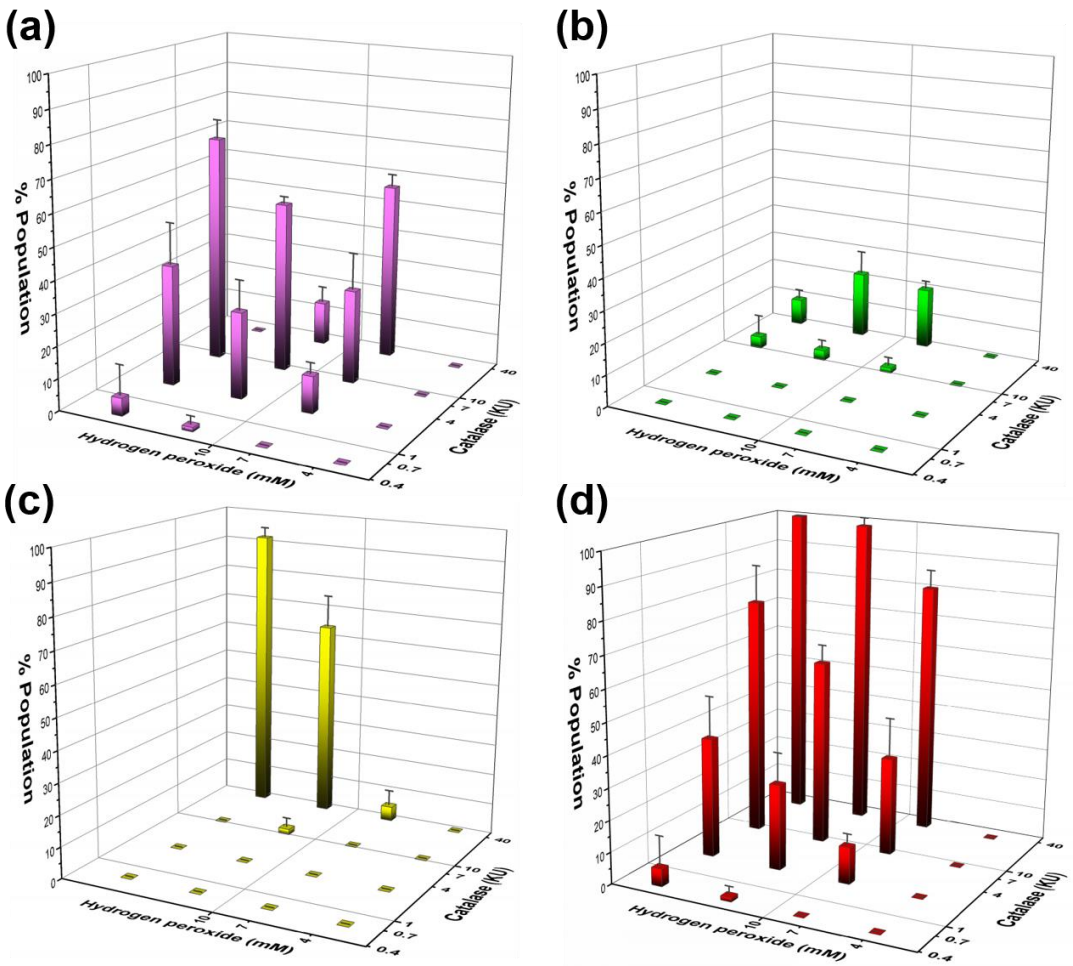

Figure 13. 3D bar graphs showing changes in the percentage of a population of organoclay/DNA microcapsules containing a single bubble (**a**), two bubbles (**b**), or three or more bubbles (**c**) as a function of catalase and hydrogen peroxide concentrations. (**d**) 3D bar graphs of the total percentage of buoyant microcapsules in the population under study. n > 15 microcapsules per experiment. n = 3 independent experiments. Error bars show standard error of mean.

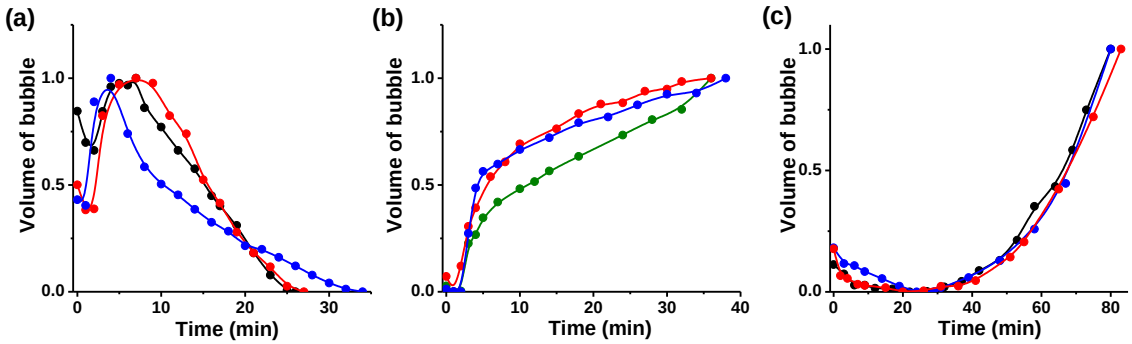

Figure 14. Normalized plots showing time-dependent changes in volume of entrapped oxygen bubbles within buoyant organoclay/DNA microcapsules (triplicates) after addition of glucose (a), sucrose (b) or water (c).

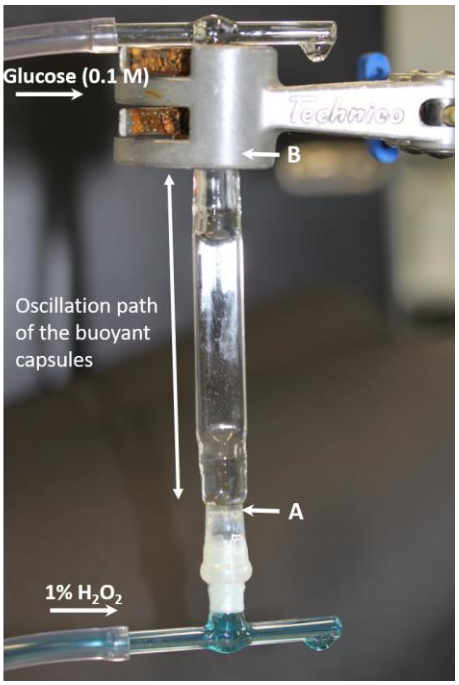

Figure 15. Photograph showing experimental set-up used to produce sustainable oscillatory movement of catalase/GOx-containing organoclay/DNA capsules. Aqueous solutions of hydrogen peroxide (1 %, stained with methylene blue (0.1 mM)) and glucose (0.1 M) are flowed across the bottom and top of a water column containing enzyme-containing capsules to produce local gradients of the two substrates. The ends of the sample tube in contact with the flowing solutions are covered in a dialysis membrane (**A** and **B;** 10 kDa cut-off) to minimize hydrogen peroxide/glucose mixing whilst allowing slow diffusion of the substrates into the water column. The latter results in the formation of discrete zones that are rich in hydrogen peroxide or glucose at the bottom and top of the water column, respectively. As a result, oxygen bubble growth and consumption within the capsules occur at different ends of the water column to generate oscillatory buoyancy.

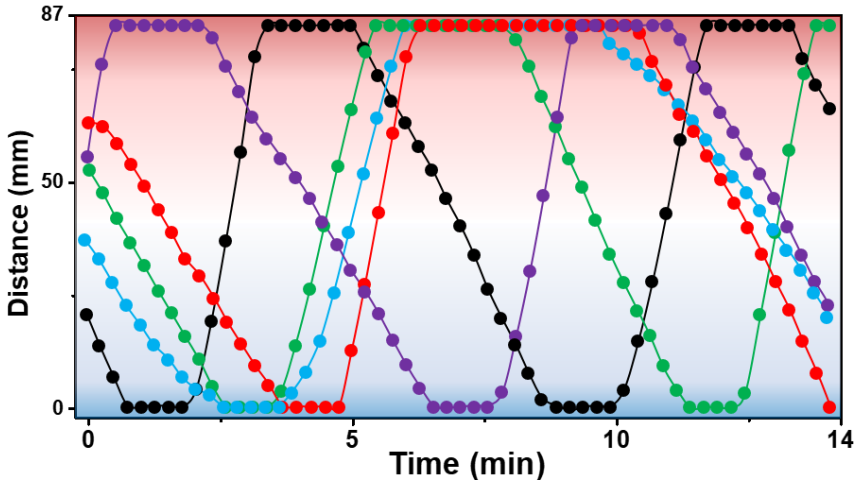

Figure 16. Plot showing time-dependent changes in vertical displacement (distance) for five organoclay/DNA capsules (black, blue, green, red, purple traces) undergoing enzyme-mediated oscillatory movement. The water column is 85 mm in length and the capsule oscillation time periods range from 8-13 min. Blue and red shading indicate the localized concentration gradients in hydrogen peroxide and glucose, respectively.

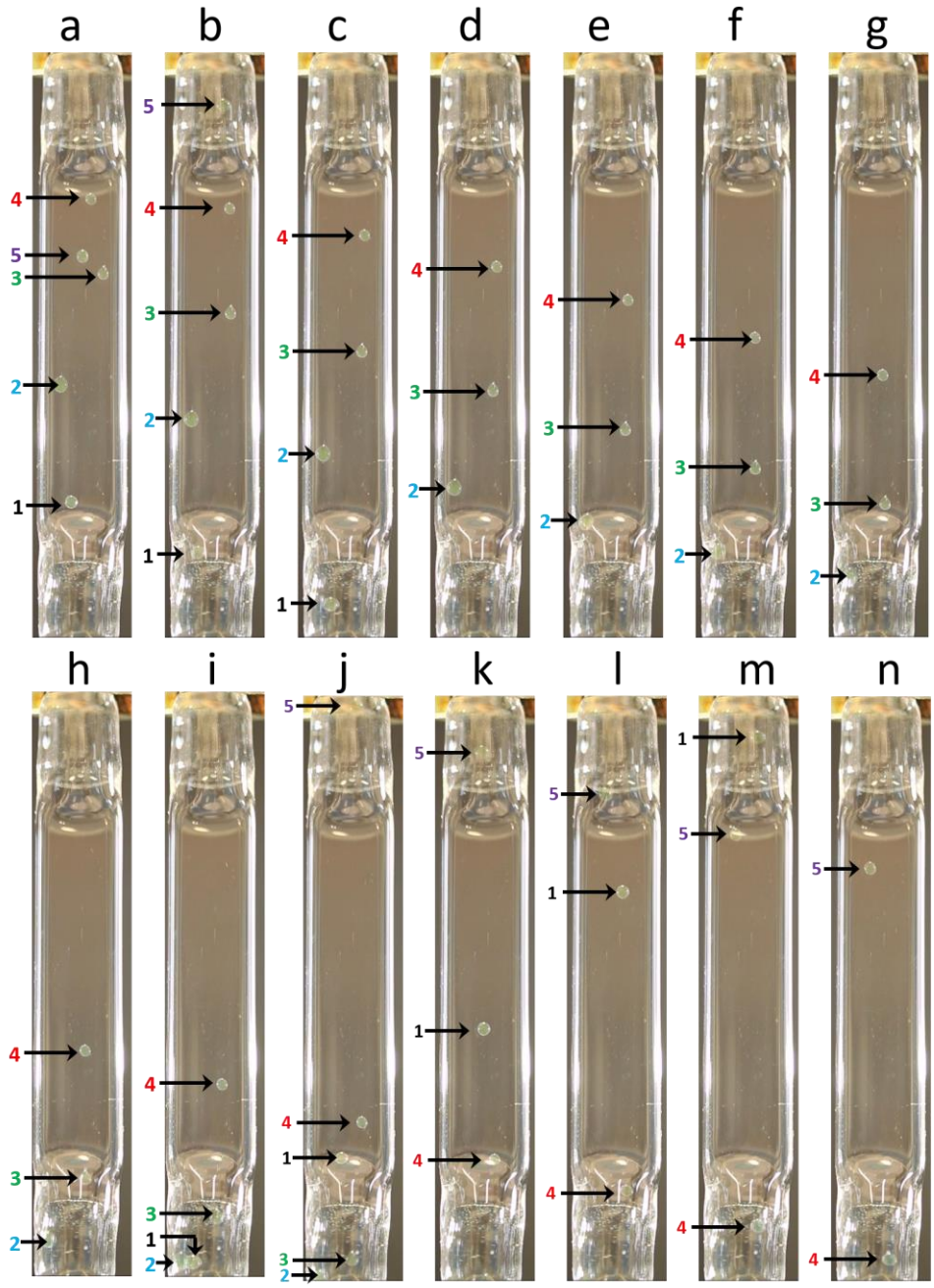

Figure 17. Time-lapse sequence of photographic images (a-n; 15 s intervals) showing oscillatory vertical movement of five catalase/GOx-containing organoclay/DNA capsules (1,2,3,4,5) arising from spatiotemporal responses to antagonistic bubble generation and depletion at the bottom and top of the water column, respectively. Initially, capsules 1-4 are in the descent phase of their oscillation (a-g), whilst capsule 5 is ascending (a,b). All capsules show a residence time at the bottom or top of the water column due to the lag time associated with the switch between oxygen generation and consumption. The speed of descent is slower than that for ascent; (compare capsule 4 (descending, (a-n)) and capsule 1 (ascending, i-m).

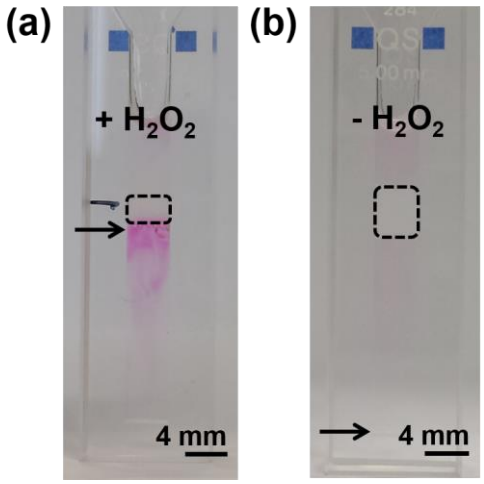

Figure 18. (a,b) Photographs of cuvettes containing a PPBP-containing agarose gel (dashed box) and catalase/ALP-containing buoyant organoclay/DNA microcapsules (arrows) recorded 5 minutes after adding hydrogen peroxide (**a**), or in the absence of hydrogen peroxide (**b**). Diffusion of phenolphthalein (pink) into the solution below from the microcapsules is observed in (**a**) but not (**b**).

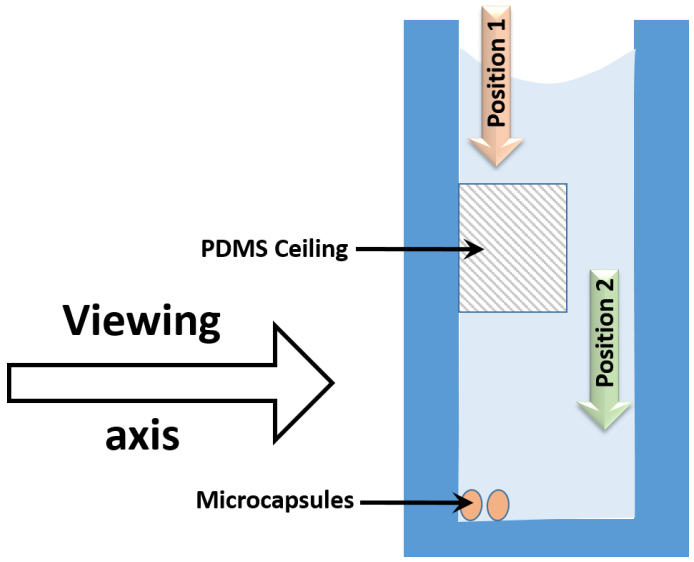

Figure 19. Scheme illustrating the experimental setup used to observe the vertical locomotion of buoyant organoclay/DNA protocells. Positions at which substrates were added into the medium are also shown: hydrogen peroxide (position 2); glucose (position 1).